Construction Robotics (2025) 9:12
https://doi.org/10.1007/s41693-025-00154-0

RESEARCH

Robotic frame winding: prefabricated fibre structures as formwork and reinforcement for digitally fabricated shell-like concrete elements

Stefan Gantner[1] · Philipp Rennen[1] · Fatemeh Salehi Amiri[1] · Tom Rothe[1] · Christian Hühne[1] · Dirk Lowke[1,2] · Harald Kloft[1] · Norman Hack[1]

Received: 20 September 2024 / Accepted: 23 April 2025 / Published online: 9 May 2025

Abstract
The integration of reinforcement in digital fabrication with concrete has led to the development of various approaches, many of which are constrained by the requirements of the concrete printing process. In contrast, the aim here was to investigate the robotic production of complex reinforcement structures as a primary process which supports the application of concrete and therefore acts as stay-in-place formwork that creates shaping potential beyond conventional printing processes. Based on the concept of combining the robotic processes of Fibre Winding and Shotcrete 3D Printing (SC3DP), the presented methodology comprised design explorations, fabrication variations, the realisation of a real-scale demonstrator and the assessment of the structural performance. Accordingly, an automated process for the fabrication of thin-shell double-curved reinforced concrete elements with controlled thickness and homogeneous concrete distribution was developed and characterised. Following this approach in the future will not only contribute to fabrication-informed design but also minimise concrete use and formwork waste.

Keywords Fibre reinforcement · Robotic fibre winding · Shotcrete 3D printing (SC3DP) · Digital fabrication · Textile formwork · Concrete shells

1 Background and motivation

In the realm of architectural design and construction, the pursuit of structural efficiency and aesthetic appeal has perpetually driven innovation. Amongst such innovations, concrete shells stand out for their remarkable strength-to-weight ratio and their ability to embody the design principle "form follows force" in reference to Louis Soullivan's famous maxim "form follows function". Historical architect-engineers like Freyssinet (Espion 2018), Laffaielle (Espion 2016), Nervi (Iori and Poretti 2013), Torroja (Antuña Bernardo 2006), Candela (Schützeichel et al. 2020), Otto (Nerdinger 2005), and Müther (Ludwig 2017) have demonstrated the vast potential of such structures, leveraging their unique shapes for both aesthetic appeal and structural efficiency. Despite their advantages, the complexity of shells has historically posed significant challenges in construction, limiting their widespread adoption. As the iconic examples of Candela's shell structures illustrate, the construction of these intricate forms often required extensive falsework and shuttering, leading to high material costs and labour demands. In contrast, Müther's 'Kurmuschel' (Fig. 1)

✉ Stefan Gantner
stefan.gantner@tu-braunschweig.de

✉ Philipp Rennen
p.rennen@tu-braunschweig.de

Fatemeh Salehi Amiri
fatemeh.amiri@tu-braunschweig.de

Tom Rothe
t.rothe@tu-braunschweig.de

Christian Hühne
christian.huehne@tu-braunschweig.de

Dirk Lowke
lowke@tum.de

Harald Kloft
h.kloft@tu-braunschweig.de

Norman Hack
n.hack@tu-braunschweig.de

[1] Technische Universität Braunschweig, Brunswick, Germany

[2] Technical University of Munich, Munich, Germany

Fig. 1 Construction process of Müther's "Kurmuschel" in Sassnitz, Germany: **a** Form-defining reinforcement structure and scaffolding; **b** Manual surface postprocessing after shotcrete application; **c** Finished pavilion today (Credit: **a**, **b** Müther Archiv—Hochschule Wismar; **c** Yvonne Kavermann, Berlin)

represented a significant innovation by reducing the need for such extensive formwork, as the concrete was directly applied to a prefabricated mesh. However, both the fabrication of the reinforcement and the application of the shotcrete were still highly labour-intensive, requiring skilled labour and careful execution. These challenges highlight the need for further innovative approaches to simplify and economise the construction of freeform shells, particularly in reducing the labour involved in both reinforcement fabrication and the concreting process.

In response to these challenges, the advent of computational design and digital fabrication technologies has opened new potentials for architectural construction. Using parametric tools, designers can integrate structural requirements and characteristics of the manufacturing methods. In addition, 3D printing has introduced the prospect of automated fabrication with unprecedented freedom of form.

The motivation of this research is to enable a fully digital design and manufacturing process for reinforced shell-like concrete elements. Given the versatility of the SC3DP (Kloft et al. 2019) process beyond layer-stacking and the novelty of continuous fibre reinforcement processed by robotic winding, this paper investigates how the combination of these two techniques can provide an automated solution to shell construction. By synergistically activating fibre structures wound in a frame as formwork for shotcrete application, the approach aims to minimise the expense and waste associated with traditional falsework and shuttering, whilst also emphasising the role of the fabrication method in defining the final form. Beyond technical feasibility, this research also considers the aesthetic potential of these methods, exploring how they can contribute to innovative architectural expressions in shell construction.

The paper is structured as follows: Sect. 2 reviews the current approaches in digital fabrication related to shell structures, providing an overview of the state of the art. Section 3 details the complete design-to-fabrication workflow, as illustrated by a real-scale demonstrator, including the iterative development of the manufacturing technique. Section 4 presents observations from the fabrication process and the resulting demonstrator, along with a preliminary assessment of the structural performance. Finally, Sect. 5 discusses the findings and insights gained, leading to the identification of opportunities for future research in Sect. 6.

2 State of the art

In digital fabrication with concrete, 3D printing plays a pivotal role. Currently, one of the most significant challenges is the integration of reinforcement within this context. However, for thin shell-like components with curved geometries, the limitations of formwork-free fabrication become dominant. Despite these challenges, various fabrication approaches exist, though they rarely cover the entire manufacturing within a digital automated process chain including reinforcement integration.

2.1 Compression only shells

3D printing avoids the additional economic and ecological costs associated with formwork. Nonetheless, overhangs that occur in shells can only be realised in special cases, such as Nubian vaults (Carneau et al. 2019, 2020). For pressure-dominated vaulted structures, a discrete assembly approach, based on the principle of the stone arch, proves advantageous (Rippmann 2016). If the individual parts are not mortared as in traditional manufacturing (Block et al. 2010), precise fabrication is necessary, hence CNC-milled stone and 3D-printed concrete casting moulds proved to be particularly suitable (Block et al. 2018; Liew et al. 2017; Ranaudo et al. 2021). Furthermore, different types of 3D-printing proved

to be applicable for segmented vaulted structures as long as precisely fitting joints are ensured (Rippmann et al. 2018; Dell'Endice et al. 2023; Nuh et al. 2022).

Despite the potential for circular construction (Bhooshan et al. 2024), the assembly involves increased effort compared to monolithic shells. These in turn commonly require a large amount of shuttering and falsework. The idea of replacing these wasteful structures with textiles dates as far back as (Veenendaal et al. 2011) and has been revisited in the context of digital fabrication.

2.2 Textile formwork in digital fabrication

For example, a textile formwork system supported by a cable net was developed for concrete shells (Veenendaal and Block 2014) and investigated in the example of the HiLo roof, a textile reinforced shape optimised shell (Block et al. 2017; Veenendaal et al. 2017). Although digital fabrication methods were not dominant, the complex shape could only be realised through digital fabrication-informed design, whereby the deformation of the cable net under the load of fresh concrete was taken into account (Méndez Echenagucia et al. 2019; Mele and Block 2010). Regarding reinforcement, the choice of flexible carbon fibre mats enabled shape adaptation, but required small patches, as they can only be bent in one direction, and sufficient overlap of single patches (Méndez Echenagucia et al. 2019).

Whilst relying on manually assembled cable-nets or bending active rods, the Knitcrete technique extends digitalization to the fabrication of textile stay-in-place formwork by deploying CNC-controlled knitting machines (Popescu et al. 2018, 2019). Knitting patterns are generated from the target geometries and can include intricate details like pockets to generate ribs (Popescu et al. 2021) or channels for the insertion of metallic or textile reinforcement (Lee et al. 2023). However, the elasticity of knitted fabric requires an additional step of stiffening through cement-paste coating (Popescu 2019).

These examples illustrate that sprayed concrete is especially suited for one-sided textile formwork. The process is open to different materials, as demonstrated by spraying clay on organic textile structures. The use of drones in fabricating small shelters has opened innovative automation potential (Chaltiel et al. 2019). In addition, robotically controlled shotcrete offers new forms of expression for surface articulation (Rennen et al. 2023a; Ercan Jenny et al. 2020, 2022).

2.3 Reinforcement integration in additive manufacturing with concrete

Regarding the automation of partial processes, besides formwork creation and concreting, the integration of reinforcement must be considered (Kloft et al. 2020a, 2024; Mechtcherine et al. 2021). For thin-walled elements, textile reinforcement is particularly suitable (Scheerer et al. 2017). Due to the corrosion resistance, materials like carbon fibres and AR-glass fibres can be used with minimal concrete coverage. The flexibility of the fibres has proven advantageous for the integration in digital fabrication processes with concrete. Individual fibre strands can be inserted simultaneously during the extrusion of concrete, which has been broadly investigated in the field of additive manufacturing (Mechtcherine 2020; Caron et al. 2021; Demont et al. 2021, 2022; Neef and Mechtcherine 2022; Neef et al. 2022). Regardless of the choice of materials, this method can even be used to expand form freedom as the incorporated fibres directly increase the tensile strength of the extruded concrete (Caron et al. 2023; Yang et al. 2023).

Furthermore, textile strips can be inserted between layers (Nikravan et al. 2023; Janse van Rensburg et al. 2022), where flexibility allows orientation along the force flow (Dörrie and Kloft 2022). The lateral application of carbon fibre meshes to 3D-printed components and their integration by means of a concrete cover has been tested in Yang et al. (2023), Nikravan et al. (2023), where the meshes are either suspended from anchors placed during the core printing or the meshes are simply pushed into the still malleable core. To extend the limited adaptability to doubly curved geometries, the drapability of textile reinforcements is being explored in Dittel et al. (2017), Bhat et al. (2022) by comparing different binding types and introducing a corresponding drape test. Unrestricted shape adaptation paired with individualised fibre orientation along the force flow was enabled by the Core-Winding-Reinforcement method (Gantner et al. 2022a). Conceptually, an individualised orientation is achievable with Tailored Fibre Placement (Tsarkova et al. 2023).

2.4 Structural stay in place formwork

If the reinforcement structure is set as the starting point of fabrication, a synergistic use as formwork can be achieved, as evidenced by the Mesh-Mould technique in the example of steel-reinforced wall elements (Hack 2018; Hack et al. 2020). Using reinforcement as support for concreting has been investigated as well for thin walled textile-reinforced concrete components. Both robotic extrusion and spraying of concrete on manually shaped and in addition supported carbon fibre meshes were tested as a feasibility study (Ayres et al. 2019; Taha et al. 2019). Flexural tests on glass fibre meshes with robotically extruded concrete revealed good bond properties (Dittel et al. 2023a). To achieve controlled embedding depth and surface quality on the back of the reinforcement mesh, the method was extended by a robotically guided sliding formwork. Here, no structural disadvantages were observed compared to cast samples, however

the surface quality was not yet flawless (Dittel et al. 2023b). Another variant of this approach is aimed at 3D spacer fabrics, whereby one of the layers should have sufficiently narrow meshes to achieve a textile shuttering effect (Neef et al. 2023).

Still, the realisation of complex doubly curved concrete elements through form-defining fibre reinforcement has been limitedly addressed in research. Compared to uniform meshes, the winding of fibre strands offers enhanced potential for shaping, including individualised orientation without generating offcuts. Beyond its application in concrete construction, the "Coreless Filament Winding" technique stands as a compelling proof of the capabilities for robotic generation of complex geometries with minimal need for support structures (Prado et al. 2014; Solly et al. 2020). Various large-scale examples demonstrate its applicability in construction (Doerstelmann et al. 2015; Solly et al. 2018; Prado et al. 2017; Bodea et al. 2020). Since fibres are particularly suitable for tensile loads, integrating them with compressive strength concrete opens up a wider application range. Initial attempts to use robotic winding for the production of reinforcement cages have left aside concreting so far (Oval et al. 2020; Friese et al. 2023; Mechtcherine et al. 2019).

The prototype presented in Schinegger et al. (2020) is an exception, in which an experimental fibre structure was coated manually using shotcrete. Due to the redundantly high quantity of fibres and the high-loss spraying process, this prototype is not of structural or economic relevance, but in line with the title 'Becoming structure', it lays the conceptual basis for using Fibre Winding as a generative process. The present paper goes one step further, contributing to a research project investigating the synergy between Fibre Winding and additive manufacturing with concrete (Gantner et al. 2022b; Hack et al. 2021). For the first time, the process is expanded to include textile formwork for SC3DP, enabling the fully automated production of thin reinforced concrete elements with minimal production waste.

3 Methods

3.1 Design exploration: learning from manual fibre winding

To explore the formal design space of the Fibre Winding process, a design studio was taught in fall 2022. The task was to investigate the potential of digital fabrication techniques, specifically focussing on Robotic Fibre Winding, to generate reinforced shell-like concrete elements. The objective was to understand the structural and formal implications of various fabrication methods, culminating in the design and construction of a small pavilion.

Students were introduced to digital design and manufacturing processes, including laser cutting, 3D desktop printing, and CNC milling. These skills laid the groundwork for experimental exploration, particularly in manual Fibre Winding at the model scale. According to the concept of Frame Winding, a set of edge curves is specified and constructed as a frame with pins so that a fibre strand can be wound over the frame in a targeted sequence, thus generating surfaces and structures.

Working in groups, students engaged in iterative design refinement informed by experimentation and computational skills. Initially, each group presented individual designs based on their model-building experiences (see Fig. 2). Important insights gained from this are that crossing fibre strands do not always touch each other and can thus form volumetric regions and that the winding sequence can produce a variation in mesh density varying from large gaps to dense clusters.

Through collaborative efforts, groups merged their results to a final pavilion design inspired by Müther's "Kurmuschel" (Fig. 1c) and built it manually on a model scale (Fig. 3a, b). This process involved analysing the strengths and weaknesses of each iteration, focussing on suitability for robotic fabrication. The culmination of this phase was a comprehensive design catalogue documenting critical parameters for design and fabrication. These insights, garnered from the students' collective exploration, guide future iterations and innovations in digital fabrication.

As the design was scaled up from the model to the robotic fabrication of a full-sized pavilion segment, adjustments were made (Fig. 3c). In particular, folding was introduced to increase the geometrically induced stiffness, together with further detailing to the point of feasibility. The development of methods for fabrication-oriented design with special focus on exploiting the shaping potential of Frame Winding is part of the research described in this paper.

3.2 Overview of manufacturing setup, materials and process steps

To better understand the methodology, the boundary conditions for fabrication are briefly outlined first, which encompass the research facility, the materials used and the overall process flow. The Digital Building Fabrication Laboratory (DBFL) located at the Institute of Structural Design (ITE) at TU Braunschweig, Germany, is a large-scale multi-purpose CNC facility that enables real-scale manufacturing in a prefabrication scenario. A work space of $16 \times 7.7 \times 3$ m is covered by two gantries from OMAG SpA, one of which can be used for five-axis machining, whilst the other gantry is equipped with a "Stäubli TX 200" six-axis robot arm, to be used with corresponding end effectors for SC3DP and Fibre Winding (Kloft et al. 2020b).

Fig. 2 Student models from the manual exploration of the Frame Winding method reveal a wide range of expressions

Fig. 3 **a**, **b** Small scale model of preliminary design; **c** Refined design for fabrication with Robotic Fibre Winding in real scale

All applications described here were performed with the same machinery and the same types of material. The reinforcement strand for Fibre Winding is continuously produced by the Dynamic Winding Machine (DWM) described in detail in Rothe et al. 2023a. Here, a 9600 tex E-glass fibre roving and L-285 epoxy resin for impregnation were chosen, resulting in a cross section of 3 mm diameter. A twisted glass fibre yarn (EC-9, 3 × 136 tex, S135) was selected for helical surface profiling. The resulting strand was optimised for use as reinforcement in concrete components (Rothe et al. 2023b). For SC3DP, a fine-grained polymer-modified cement–based concrete (Nafufill KM 250, MC Bauchemie) is processed by a setup consisting of a "WM Jetmix 125″ mixer, a "WM VarioJet FU" concrete pump and a DN/ID 35 hose of 25 m length.

Considering the fabrication setup, the pavilion segment was placed in rotated orientation within the build space for better accessibility circumventing limitations on component height. The fundamental fabrication strategy depicted in Fig. 4 involves Fibre Winding over a pre-installed frame, creating both a reinforcement structure and a formwork surface for the subsequent shotcrete application. To embed the reinforcement from both sides, the backside was planned to be concreted after removing the frame structure. The critical factor for successful implementation is enabling the fibre structure to act as formwork, as detailed in the following investigations.

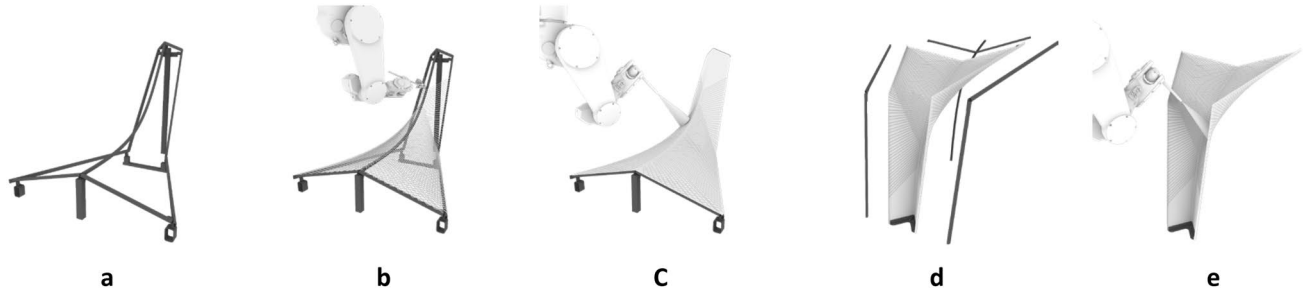

Fig. 4 Process steps: **a** Frame assembly; **b** Robotic Fibre Winding around pins with simultaneous tape placement; **c** SC3DP on textile formwork; **d** Flip, erect and detach frame from the cured structure; **e** SC3DP on the other side

3.3 Preliminary studies on fibre meshes as formwork for shotcrete

In previous attempts to functionalise fibre reinforcement as formwork for shotcrete, the primary challenge proved to be concrete flying through the mesh (Hack et al. 2021). It was considered unlikely that overshooting material could be prevented solely by modifying its rheology, as the scope for flowability changes in the spray setup is limited. Instead, two different strategies were pursued to capacitate meshes as formwork: Either an external mobile formwork could hold the material in place or the mesh could be densified to prevent material transition in the first place.

3.3.1 Shield printing approach

The first approach requires two robotic systems, so that shotcrete is applied from one side onto a reinforcement structure, whilst the same trajectories are traced synchronously on the back with a shield (Fig. 5a). This CNC-controlled slip formwork was intended to not only stop excess material but also produce a smooth surface. In the course of a test series on flat, vertically installed fibre meshes, no satisfactory results could be achieved, whereby two main problems could be identified. Firstly, a thorough penetration was not obtained in any configuration, leading to voids between the mesh and the shield (Fig. 5b). Secondly, there was always permanent concrete deposits forming on the shield.

Several attempts have been made to avoid this behaviour. Varying the shield material between steel, PTFE and printed PLA had only minor influence and could not prevent perpetual accumulation of concrete on the shield. Static and rotational movements always led to material deposition on the shield being dragged along the pathway, leaving defective traces behind. By using a vibrating shield, the adhesion problem was solved at the cost of uncontrolled material flow behind the shield area. Regardless of the potential chance to achieve a non-porous undisturbed material deposition through further investigations, this test series suggests limited geometric freedom due to the planarity of the shield

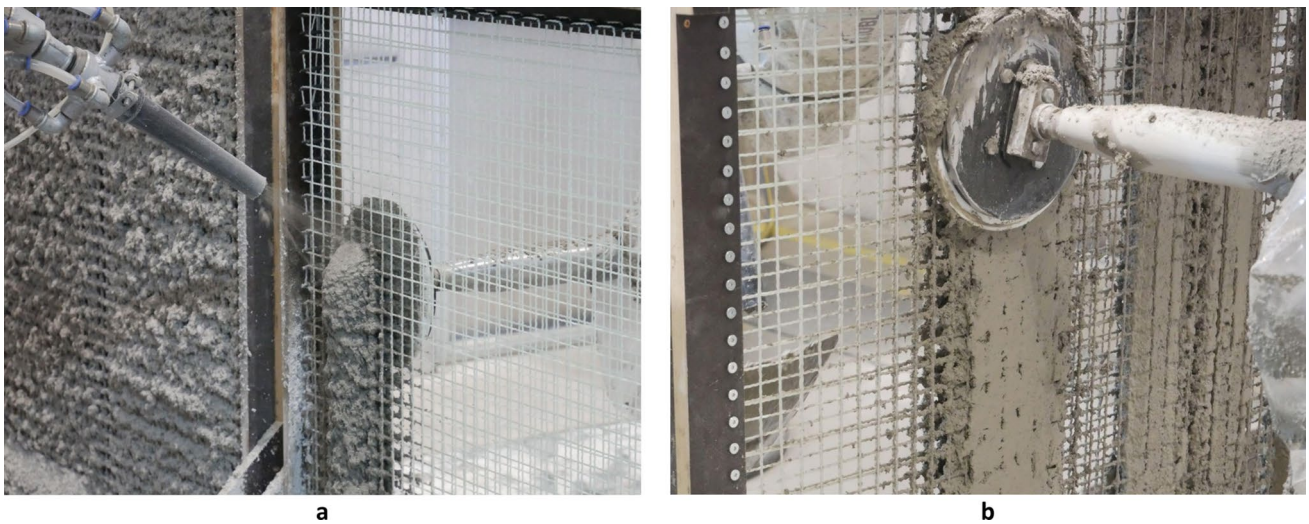

Fig. 5 **a** Shotcrete Printing on vertical mesh with synchronised CNC-controlled PTFE-shield on the rear side; **b** Smoothed concrete surface with defective voids

formwork. Consequently, a different concept of utilising the mesh itself to act as formwork was followed.

3.3.2 Sprayed short fibres approach

Similar to the approach of Robotic Aerocrete (Taha et al. 2019), the concurrent spraying of glass fibre cuttings and concrete using two distinct nozzles was tested for its ability to minimise excess material. The study involved spraying onto flat vertical fibre meshes of sizes from 15 to 30 mm from distances of 20 cm, 30 cm, and 40 cm, with nozzle orientation orthogonal to the mesh (Fig. 6a). The adjustable fibre length was set to 62 mm to ensure exceeding the mesh sizes.

Initial tests determined the optimal arrangement of the fibre nozzle relative to the shotcrete nozzle, in terms of their positioning along the direction of travel. It was observed that the spray cones from each nozzle did not fully intermingle, resulting in the fibres being deposited either beneath or atop the concrete layer. Opting for the former configuration was deemed favourable for mesh coverage. A control test, conducted without sprayed fibres, revealed a significant overshooting of concrete, leaving only a thin coating on the fibre strands of the mesh. When incorporating sprayed fibres, they formed a barrier between the mesh and concrete, leading to immediate delamination.

The fibre flow rate was reduced from 380 g/min to the spray gun's lower operational threshold of 280 g/min in an attempt to mitigate this issue. Following the adjustment, the material exhibited improved adhesion to meshes sized 15 and 20 mm. Conversely, for mesh sizes of 25 and 30 mm, the sprayed layer partially peeled off (Fig. 6a), indicating a persistent separation effect, which was also confirmed by sectional imaging (Fig. 6b). Moreover, all mesh sizes exhibited insufficient continuity in the formation of a closed concrete surface. On average, the rate of excess concrete ranged from 28% for the 15 mm mesh size to 64% for the 30 mm mesh size, across the three tested nozzle distances.

An additional experiment tested whether applying a preliminary layer of sprayed fibres onto a mesh pre-impregnated with wet epoxy resin would enhance outcomes. However, this approach resulted in poor fibre adhesion to the mesh, with a significant quantity being displaced during shotcrete application, leading to even higher excess material rates of 60–80%. This investigation reveals the limitations of using sprayed fibres and shotcrete as a means to enable meshes as formwork. The separation caused by the fibres compromises the bonding between concrete and mesh, meanwhile the issue of excess material remains partly unresolved.

3.3.3 Tape laying approach

Inspired by textile formwork and Automated Tape Laying (ATL) (Crosky et al. 2015), we devised a further approach to enhance formwork functionality within fibre wound reinforcement structures. This method aims to reconcile the need for a discrete boundary surface to prevent concrete from flying through the mesh with the requirement for a material that promotes effective bonding to the concrete. Glass fibre fleece tapes, commonly used for crack prevention in drywall construction, emerged as a suitable choice for this application, offering the necessary balance between density and porosity. Its thin, yet dense structure allows for concrete application from both sides without compromising on bonding quality.

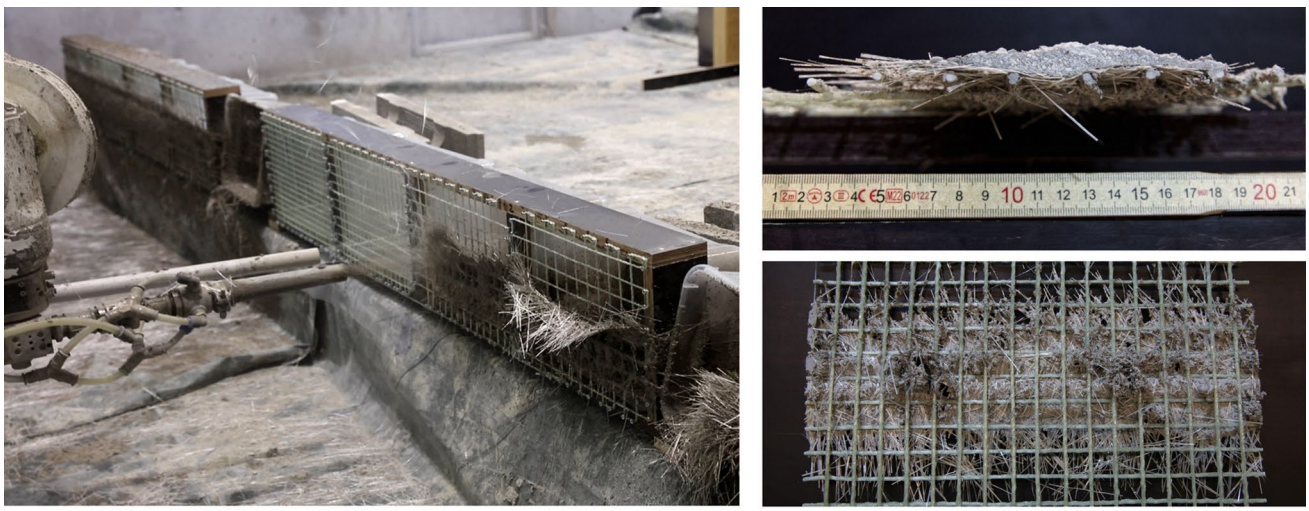

Fig. 6 **a** Concurrent spraying of short glass fibres and concrete on fibre meshes; **b** Formation of a separation layer of short fibres visible in sectional image (top) and in rear view (bottom)

A detailed view of the selected tape ("catnic Fugenbewehrstreifen") of 50 mm width and 0.3 mm thickness is given in Fig. 7b.

Leveraging the individualised nature of the winding process, the fleece tape is intended to be deposited concurrently with the fibre strand, allowing to situate the tape between two layers of a grid. This integration aims to establish a formwork layer without the need for additional process steps. A preliminary proof of concept was conducted manually on a double-curved surface, revealing the tape's ability to accommodate torsion and overlapping without compromising its integrity (Fig. 7a). Despite the dry assembly, the tape was held in place by a notable clamping effect amongst the fibre layers. Acknowledging the manual process's complexity, an end effector prototype was developed to automate the application of glass fibre fleece tape within the winding process.

3.3.4 Development of end effector for tape laying

Compared to ATL processes known from fibre compound structure production, the integration of fleece tape into the Fibre Winding process comes with different requirements. Instead of a solid prefabricated formwork, the fleece tape is supported only by an initial layer of fibres. By depositing the fleece tape together with a second crossed fibre layer, it is being fixed in place and thus does not need any instant glueing like in ATL. As the fibre strands are impregnated with cold-curing resin, further consolidation of the fleece is expected in the course of curing.

Unless combined with the winding process, an active drive is required to deposit the tape. Here, a passive drive can be implemented, building up on the robotic end effector for Fibre Winding, which, in essence, is a simple tube for redirecting the fibre strand. The direction and speed of the outgoing strand is determined solely by the movement of the robot arm. The key of the tape enhanced end effector lies in a mechanical transmission of the fibre movement onto the fleece tape. Hence, the only active control needed is a start-stop-mechanism that allows to feed the tape to the strand and to cut it at arbitrary positions.

Figure 8 gives an overview over the components of the prototype end effector. The primary structure for winding consists of a tube equipped with freely orientable pulleys on both ends. Meanwhile both pulleys assure a damage free redirection of the fibre strand, the bottom pulley in addition serves as base for the entire fleece-tape-unit, so that it would always align with the outgoing fibre strand. It comprises a drum for the tape-roll, a feeding channel and a cutting unit.

The feeding channel has nozzles incorporated that allow conveying the tape from the cutting unit to the pulley by means of compressed air. At the point where the tape encounters the pulley, a spring-loaded flap is installed, which is supposed to transmit the movement of the fibre strand onto the fleece tape. Like this, the robot arm can pull out the fibre strand, which in turn pulls out the fleece tape. Attention was paid on balancing the weight of the fleece-tape-unit around the tube and on avoiding friction in such a way that the passive alignment with the fibre strand works independently of the spatial orientation of the end effector.

Air-pressurised solenoid valves, which are integrated in the robot arm, could be used to incorporate digital commands for cutting and feeding tape. With this control system, the end effector is capable of either depositing the fibre strand only, or adding the fleece tape to it. Test runs on simple mesh geometries confirmed the operability. Apart

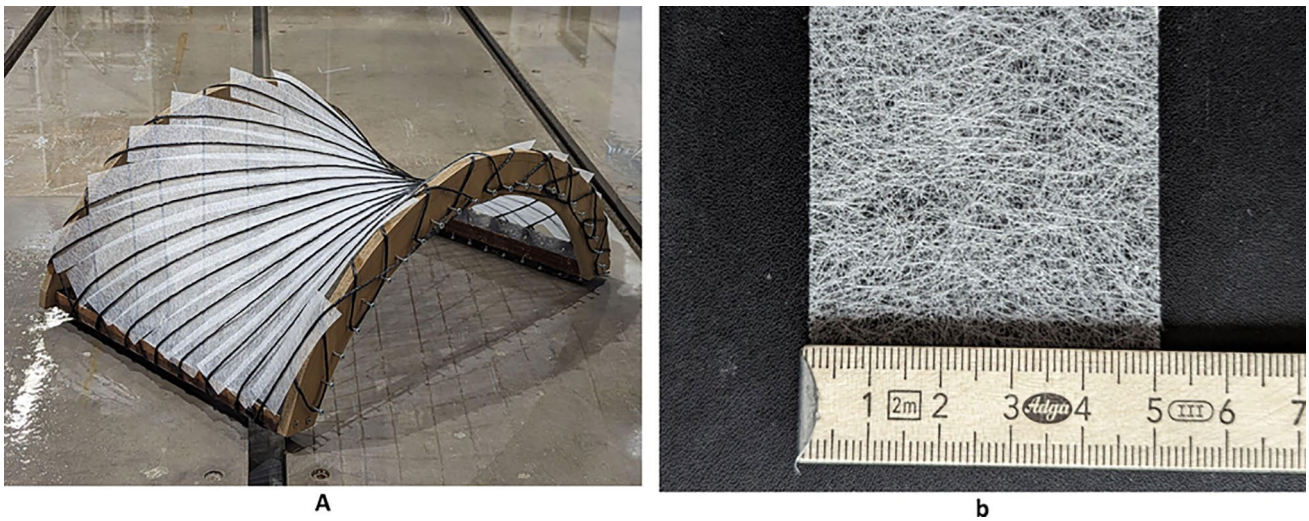

Fig. 7 **a** Manual proof of concept for the integration of fleece tape in a double-curved winding structure; **b** Close-up view of the selected glass fibre fleece tape

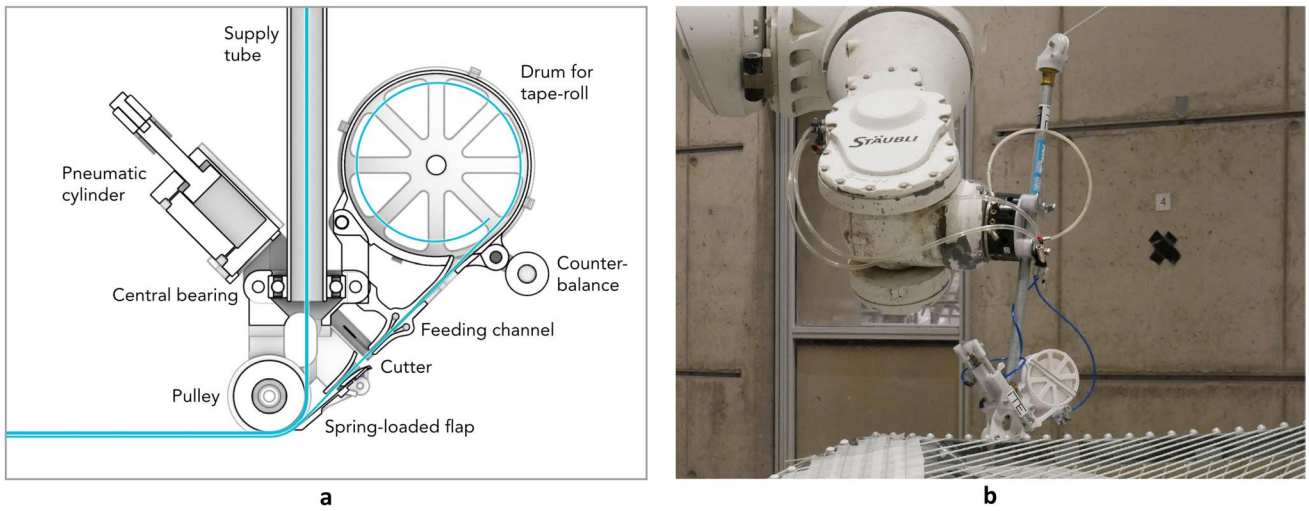

Fig. 8 **a** Detailed section drawing of end effector for tape laying and winding; **b** Full end effector including inlet for reinforcement strand and flange to robot arm

from the reliably functioning alignment and cutting, the interaction between the air-driven and the passive conveying mechanism proved to be difficult to tune, but was initially retained for the demonstrator fabrication without significant modifications.

3.4 Methodology frame winding

The overarching goal of using Frame Winding to generate an integrated structural stay-in-place formwork for concreting entails certain requirements. The following requirements have been derived both from the experience of the exploratory student work on the Fibre Winding process (Sect. 3.1) and from the preliminary studies on the robotic concreting of fibre meshes (Sect. 3.3).

Requirements for Fibre Winding formwork:

- Continuous surface creation;
- Homogeneous mesh distribution;
- Minimal use of frames;
- Sufficient stiffness of frame and fibre mesh.

Design explorations towards intricate geometries revealed that winding onto a frame can lead to the appearance of non-intersecting strands forming a volume. However, for reliable use as formwork, a thin continuous surface without volumetric artefacts is targeted. Furthermore, the density in wound fibre structures can vary from large openings to bulky agglomerations of fibre strands. However, retaining fresh concrete and integrating the fleece tape is facilitated rather by a homogeneous fibre distribution. The frames are integral to the formwork system, but not to the fabricated elements. Their deployment should therefore be kept to a minimum, whilst ensuring adequate stiffness to support fresh concrete with negligible deformations.

The design and manufacturing aspects must be considered simultaneously when developing a fabrication system, to avoid limiting the applicability to complex geometries. Therefore, a specific real-scale demonstrator was selected as a design task, facilitating the mutual development of design and robotic realisation. Meanwhile the design was already explored experimentally by students on a model scale (Fig. 3a), a more detailed investigation was undertaken in the following.

3.4.1 Form finding and geometric simulation

A simulation of Fibre Winding structures is essential for an efficient form finding procedure. Ideally, a designer can define a set of curves representing frames and retrieves shapes of fibre structures as an outcome of a simulative algorithm. However, the winding syntax as the sequence of pins to be connected by a fibre strand offers an immense number of variations. With help of the previously defined requirements, a reduction to a standardised solution with a manageable set of control parameters is possible.

To create a homogeneous mesh where the size of the openings varies as little as possible, it is an obvious choice to use regular patterns. For planar cases, it is known from the field of tessellation that the number of patterns formed by continuous lines is limited. Square grids are particularly advantageous because squares have a small perimeter compared to their area, which implies low fibre consumption. Regarding practical implementation, a two-layer orthogonal structure of the grid also facilitates the integration of the formwork fleece tape.

When attempting to transfer planar square fibre meshes onto spatially arranged frames, uniformity and orthogonality can no longer be strictly adhered to. Through a heuristic construction principle, a minimal deviation from the ideal distribution is sought. By specifying a target mesh size, lines can be drawn across the frame that are pairwise approximately parallel. A second set of lines can be aligned to be approximately orthogonal to the first set.

As soon as fibres from different layers overlap, a simulation of the deposition behaviour including the fibre interaction becomes necessary. A detailed physical simulation of the fibres was deemed impractical, as not all the required parameters such as the modulus of elasticity of the fibre strands and the winding tension are known during the form-finding process. The fibres were therefore approximated as non-elastic. As long as the actual stiffness is high compared to the winding tension, minor deviations from the geometric prediction are expected.

This simplifies the simulation to the extent that fibre strands that have already been laid down are no longer changed by new fibre strands. Neglecting self-weight, free strands span into a line between the corresponding anchor points. Once fibres are crossing on top, they might be deflected. Assuming frictionless interaction, such a strand spans along the shortest possible path, which represents a geodesic. In detail, however, this is only partially true: If a fibre strand spans over an elevation, the geodesic curve describes its course. However, the fibre strand will not follow a valley, but will span it in a straight line.

Meanwhile the research on shortest-path-problems offers a range of different solutions, a simple algorithm termed "midpoint method" (Baek et al. 2007) or "short ruler method" (Stadler 2014) has been chosen, as it is easy to implement and to modify. Starting from an initial guess, it shortens a curve iteratively on a 3D surface so that it converges to a geodesic. The curve is approximated as polygonal line. By connecting the midpoints of its segments, a new polygonal line is formed in each iteration. To assure that this path remains on the surface, the respective closest points from the midpoints are calculated.

With help of an orientation vector as additional input parameter pointing towards the side, from which the Fibre Winding will be applied, the algorithm could be adapted to better simulate the fibre behaviour. The vector from a midpoint to its closest point on the surface is compared to the input vector to find out whether the midpoint lies before or behind the surface. Only if the midpoint is located behind the surface, it is replaced by the closest point on the surface. Like this, the path sticks to convex areas, but forms a straight span over concave areas.

The simulation can now support the form-finding process to not only retrieve a homogeneous mesh, but also to detect volumetric regions in which fibre layers are separated from each other. Besides the orientation of the first set of lines across a frame, the order of deposition has proven to be a decisive factor in avoiding such areas, which is illustrated in the following based on the selected frame geometry.

To determine the order of fibre placement, the frame was first filled with quasi-parallel lines. A loft was used to generate a surface on which the simulation of the second crossed fibre layer was carried out. Comparing Fig. 9a and b reveals how the inclusion of fibre interaction helps to predict where volumetric regions can be avoided (magenta) and where they remain (cyan). Figure 9c illustrates that the first layer is only deployed in areas where the second layer rests on the first one, excluding the cyan area in Fig. 9b. Here, the second layer takes over the role of the first one in defining the shape.

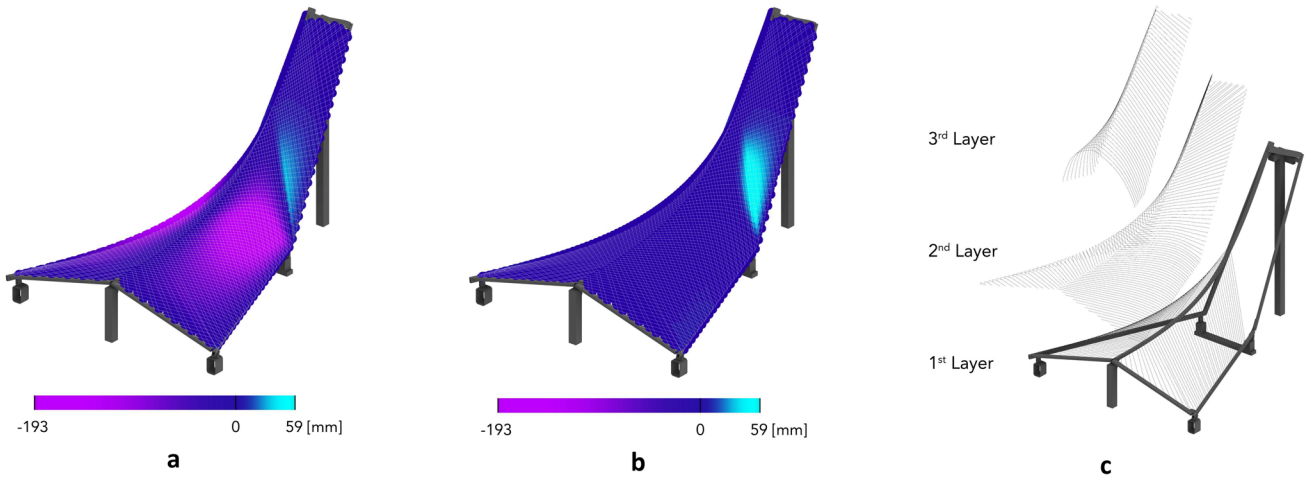

Fig. 9 **a** Distances between 1st and 2nd fibre layer without interaction; **b** Distances, when 2nd layer is laid on top of 1st one; **c** Final distribution into three layers avoiding volumetric regions

The orientation and extent of a third layer were selected so that it rests on the second layer and is nearly orthogonal to it.

In parallel, the distribution of the anchor points had to be adapted to the case. Equidistant spacing was chosen along the long sides. The distribution on the short sides was adjusted so that the fibre strands remain approximately parallel. Multiple assignments of points to several layers were taken into account.

The creation of a surface from a given frame contour is therefore not a deterministic process, but rather an iterative procedure in which different starting configurations may have to be tested to find a satisfactory shape and to fulfil boundary conditions leading to a sheet-like, non-volumetric homogeneous mesh. In the final step of form finding, a comprehensive surface was interpolated from all fibre curves, which formed the basis for robot path planning and for detailed planning including the actual frame and pin dimensioning.

3.4.2 Frame geometry and construction

In the following, the frame system for the demonstrator is described with a focus on generally applicable aspects. Conceptually, the frame could be regarded as integral to the fabricated element, implicating all resource and manufacturing efforts count to the element. Instead, it was investigated whether this impact can be avoided by removable and thus reusable frame elements.

For straight sections, rectangular steel profiles have been chosen as they are stiff and easy to machine (Fig. 10a). Especially in combination with stud welding, cylindric metal bolts could be placed fast and firmly along the profiles (Fig. 10c). Having all pins pointing in the same direction opens up the chance to remove the frame element later on. Sleeves 3D-printed from PETG have been designed to separate the fibres—especially the epoxy resin—from the bolts and to increase the pin diameter for a reduced risk of fibre damage.

From previous experiments it is known that fibres can easily slip off from pins whenever their direction has a component pointing in the direction of the pin away from the frame. Hook shaped pins could prevent this, but would make the frame removal harder. Instead, it is as well possible to avoid these difficulties by rotating the frame element in a position where the angle between the pin-normal and the fibres is always larger 90°.

The removability would also be given for planar curved frame elements, as long as the pins are located inside the plane. For the curved frame-segment visible in Fig. 10b in the middle of the demonstrator, welded pins would make a frame removal impossible. Instead, pins 3D-printed from PETG were screwed to the frame. The manufacturing of the curved frame element itself required far more effort compared to the straight frames which makes these preferable for design decisions.

Reversible connexions between the frame elements were designed in a way that the frames could be removed successively. T-slot Aluminium framing was used as scaffolding to set-up the entire frame structure on the robotic fabrication platform in the DBFL. Supporting each vertex of the frame can be regarded as a generally applicable way to achieve a high stiffness without the need of frame connexions with high bending stiffness. The metal base connector plate of the demonstrator has been designed individually to remain in the final piece and to distribute the forces from the floor connectors.

Prior to the manufacturing of the frame, the pin positions have been calculated, taking their actual diameter into

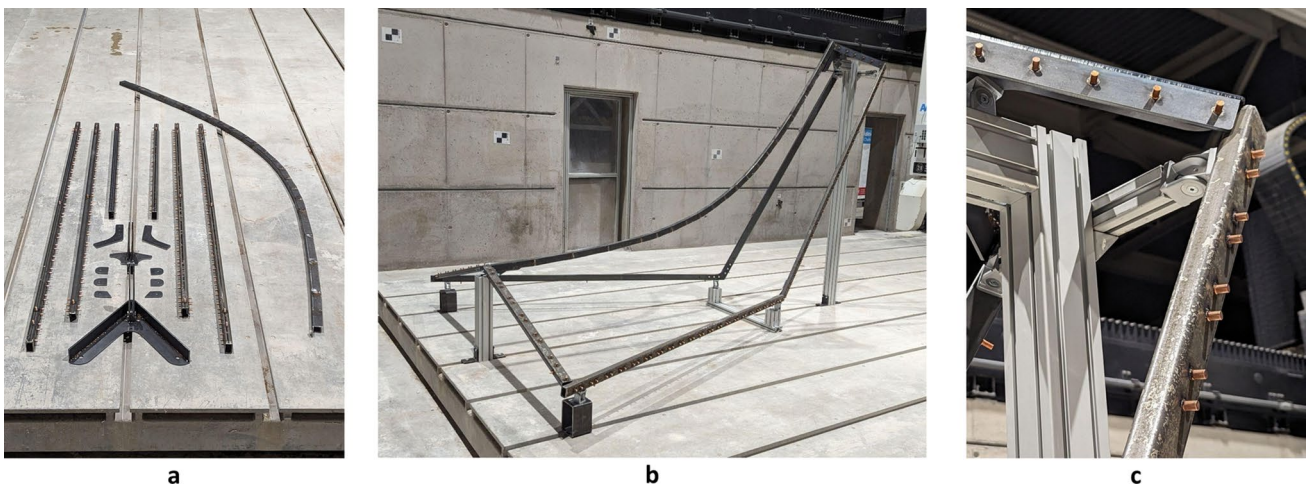

Fig. 10 **a** Individual frame parts illustrate design for disassembly; **b** Frame assembled on auxiliary T-slot framing; **c** Detailed view of assembly featuring stud welded pins

account. To preserve the uniform spacing of the fibre strands, the pins need to be placed tangentially to the intended fibre position, either on the left or right side depending on the overall winding syntax. Taking such detail into account emphasises once more the iterative nature of the design process as it requires the consideration of the robotic pathway in advance.

3.4.3 Path planning for robotic winding

Robotic path planning is different from 3D-printing or milling as the end effector trajectories do not entirely match with the final fibre position. This results on the one hand in an increased complexity as the fibre spanning behaviour needs to be considered. On the other hand, there is a certain flexibility that allows the pins to be surrounded in a collision free manner. The prediction of the fibre position serves as a base for the robot programming. For a complete path, first the single strands have to be connected to a full sequence, second a universal method for pin surrounding needs to be employed and third the control of tape laying needs to be implemented.

Meanwhile the order of fibre layers is set by the form finding, the particular sequence is not defined yet. Meandering successively through a set of uniformly aligned fibre strands is a straight-forward solution that avoids redundant fibre allocation at one spot. Like this, the strand is deflected about 180° by surrounding two pins at a time along the edges. The inner frame element redirects the strand by a smaller angle over single pins. Some of the layers cannot be deposited in a single run, but are split in two patches.

For surrounding pins, a specific routine is required to avoid collisions. The decisive factor here is not the final course of the fibres, but rather the free space between the pins and consideration of the freely orientable pulley of the end effector.

The surface from the form finding has been extended by the geometry of the frames and the simulation of single fibre strands has been repeated, resulting in endings tangential to the pins. Local coordinate systems are formed by the respective tangent vector and the pin normal, so that relative path shifts are possible with globally adjustable parameters as depicted in Fig. 11a. They allow shifting the path sideways away from the pins and extending the path over the pin by the length of the trailing pulley. In- and outcoming paths are finally connected by a line.

From manual winding experience it was found that at the beginning of the pin surrounding, the fibres can be guided over the pin instead of around it to minimise lateral shifts and thus reduce the risk of tape displacement. This technique also enabled a safe pass between the more closely spaced pins of the inner frame element.

Finally, an offset parameter was added that shifts the entire path normal to the base surface to account for the fibre thickness and to give another leverage for collision avoidance. The surface normal was also used to set the end effector orientation. As the pulley orients itself freely along the fibre strand which is visible in Fig. 11b, one rotational degree of freedom around the surface normal remains. It was used together with the redundancies given by the portal of DBFL to achieve a continuous accessibility for the robot arm.

After approximating the continuous path through single waypoints in a fine resolution, the commands for controlling the tape laying were implemented. The start of the tape feeding, its duration and the cutting are triggered via length parameters applied to each fibre segment. The respective commands are inserted between adjacent waypoints in the

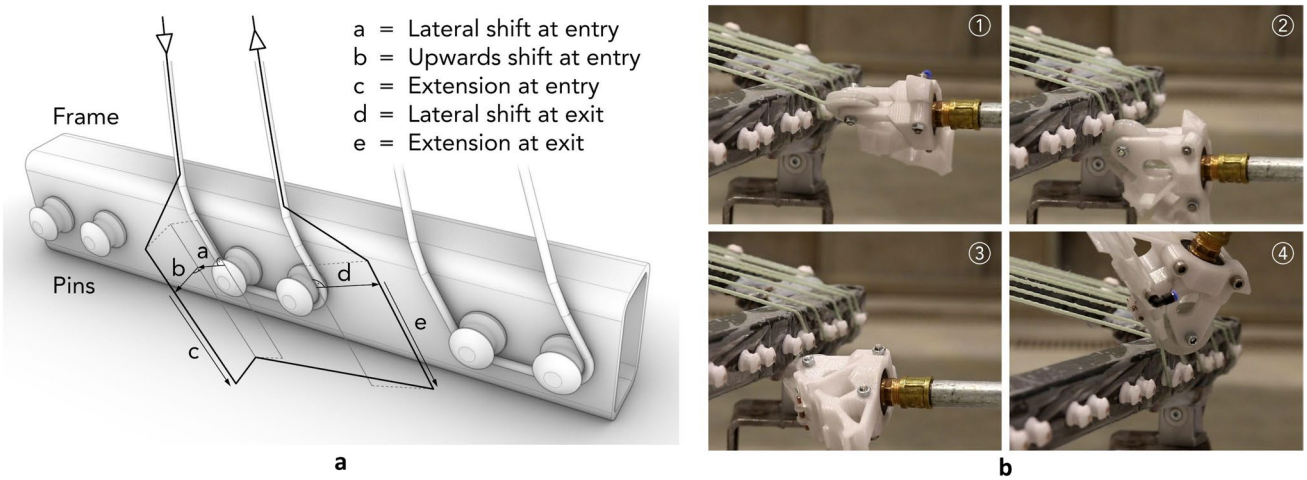

Fig. 11 **a** Parameterized path logic for pin surrounding; **b** Photo sequence of winding around a pair of pins illustrates passive alignment of the pulley

G-code, the programming language used here for robot control. As the two areas that require tape integration are overlapping, one of the two was trimmed accordingly so that the tape strips gradually become shorter, thus avoiding double allocation.

3.5 Concreting methodology

The automated, robotic concreting process for this geometrically complex and relatively fragile structure requires careful planning and preliminary tests. The focus is on the very thin application of material to the textile formwork, which is made possible by a modification of the SC3DP process towards a Robotic Area Shotcrete Printing (RASP) in which, instead of layer upon layer, large area layers are sprayed next to each other to achieve an even and very thin application of material. Although this method has already been tried and tested, this project is the first to coat a complex "poly surface", consisting of multiple double-curved surfaces, with a very thin layer of concrete of differentiated thickness. The following sections deal with the coating strategy, robotic path planning, process parameters, preliminary tests, execution planning of the SC3DP process and edge finishing through green-state CNC-milling.

3.5.1 Path planning for SC3DP

For the development of the coating strategy, the geometry was divided into two distinct groups based on their surface characteristics and concreting requirements. The majority of the surface area consists of large, double-curved surfaces, whilst the edge areas on the frame are composed of narrow, planar surfaces. These two groups necessitate different path planning strategies. The narrow frame elements, or ribbons, which are oriented along the longitudinal edges of the demonstrator, introduce a 40 mm wide crease that acts as a join partner to the neighbouring pavilion segment. Due to their structural role, these ribbons require increased material thickness and are thus treated separately, each narrow enough to be covered with a single path.

In contrast, the large-area parts of the geometry must be evenly covered with several spread-out paths, which requires a more complex strategy. For this, a tween curve operation is employed between the edge curves of the surface, projected onto the surface. A tween curve operation, also known as an interpolation or morphing curve, generates intermediate curves between two edge curves. This is mathematically represented by interpolating points along the edge curves: given two edge curves $C1(t)$ and $C2(t)$, where t is the parameter, the tween curve $C(t,\alpha)$ at an interpolation parameter α (where $0 \leq \alpha \leq 1$) is defined as

$$C(t, \alpha) = (1 - \alpha)C1(t) + \alpha C2(t)$$

This ensures a smooth and continuous path between the two edge curves, enabling an even and efficient coating of the large double-curved surfaces.

To generate a G-Code out of the curves, they are divided in a variable number of waypoints, which are directed normal to the surface. With the location and direction information in place, those extracted information are sorted in a way, that follows each tween curve, with a direction switch at every second curve, resulting in a meandering motion that follows exactly the surface geometry in soft curves with sharp turning points at the end points (Fig. 12a).

As learned from the SC3DP Process of the Knitcrete Bridge (Rennen et al. 2023b), the robotic path on the surface needs to be smooth without sharp turns to achieve a constant robotic motion resulting in a uniform spray pattern. To realise an even surface quality without the need for surface postprocessing, the spray pattern needs to be precisely tuned regarding overlap. The overlap is set to 25% on each side, whilst the absolute overlap distance is dependent on the sprayed path width and is parametrically linked to it. To avoid sharp turns on the target surface area, the turning points of the meander path are extended out of the target surface by just the estimated target radius of the shotcrete path, which is also dependent and parametrically linked to the variable nozzle distance. This parameter needs to be variable to evenly cover non-rectangular surfaces, because the tween-based path planning includes non-uniform distances between neighbouring tween curves.

The varying path width of the shotcrete is most flexibly controllable by adapting the nozzle distance: the higher the distance between shotcrete nozzle and target surface, the wider the spray cone and vice versa. To achieve most homogeneous spraying behaviour, the nozzle is always oriented normal to the surface. The Knitcrete Bridge experiments (Rennen et al. 2023b) have revealed that spraying widths in a range between 80 and 240 mm can be achieved with machine parameters of 50 Nm^3/h air pressure and 0,4 m^3/h concrete flow rate, using a 12 mm nozzle (Table 1). Those boundaries are respected in the path planning, resulting in the tween curve distance from 41 to 161 mm at a tween count of 10 curves per side. To calculate the nozzle distance relative to the desired path width, the SC3DP data set published in Lachmayer et al. (2023) was used as a base line to predict the spray cone and extrapolated linearly. To experimentally verify the extrapolated values, a parametric system was developed around the path width minimum and maximum as fixed values, which correlate to unknown nozzle distance values that had to be defined in a single preliminary test path. Once these values are identified by measurements of the test path, they can be set as a fixed correlated range and remapped to the already fixed path width at each waypoint position. This

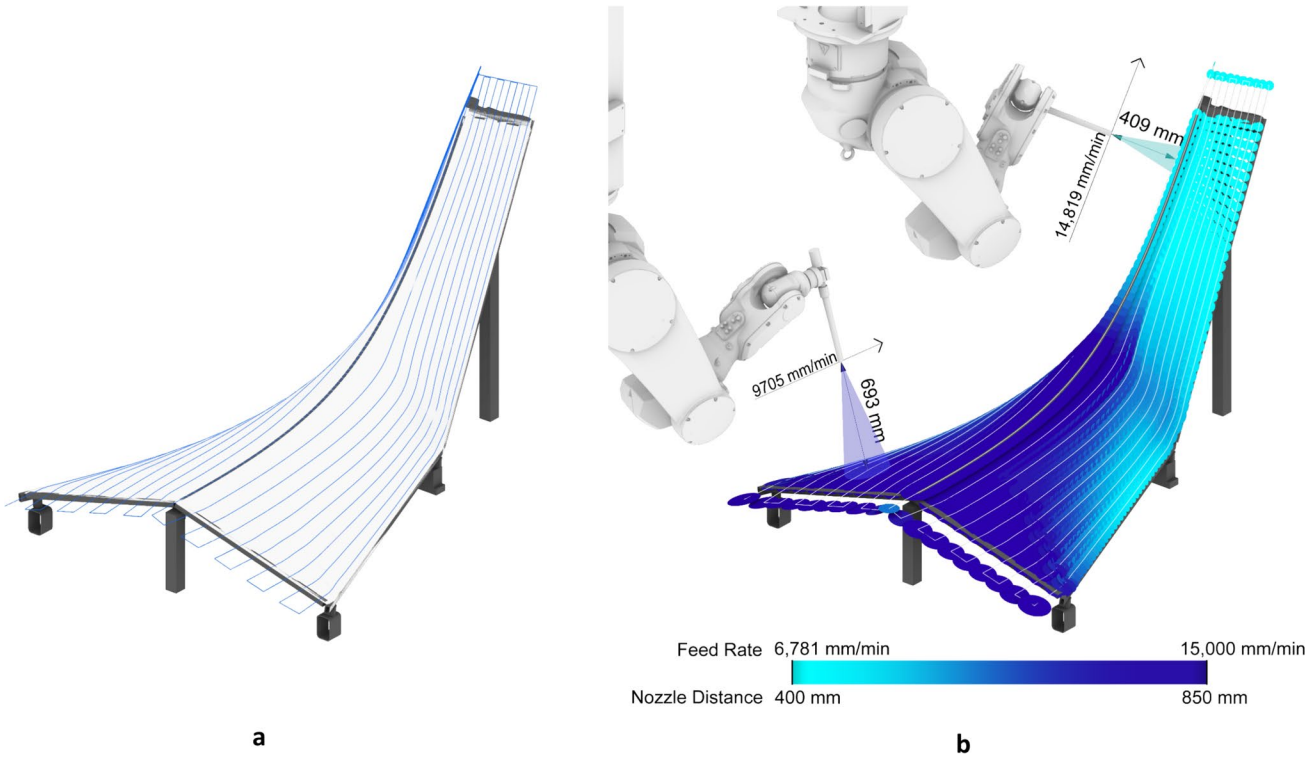

Fig. 12 **a** Path planning base curves morph from edges to mirror axis; **b** Nozzle distance and feed rate correlating to path width

Table 1 List of relevant parameters for SC3DP and RASP path planning

Parameter	Thin and large surface areas	Thick and linear ribbons
Feed rate [mm/min]	6781–15,000 (variable)	4000 (constant)
Nozzle distance [mm]	400–850 (variable)	200 (constant)
Concrete flow rate [m3/h]	0.4	0.4
Air flow rate [Nm3/h]	50	50

distance data set, ranging from 400 to 850 mm, is then used to move all the waypoints from their surface origin to the final offset position (Fig. 12b).

Through the nozzle distance shift, the amount of applied material would vary accordingly: the closer the nozzle—the higher the material build-up. To compensate for this, the material flow rate or the robot feed rate are possible parameters that need to be parametrically adaptable to the nozzle distance. Due to inertia effects, a delayed response behaviour is to be expected when dynamically adjusting the flow rate. Therefore, it is more reliable to keep the concrete flow rate constant and adapt the latter parameter of robot feedrate.

The feed rate is modulated from the robot's maximum feed rate of 15,000 mm/min at areas of most narrow path width, down to about one quarter of the maximum feed rate, which translates to 3324 mm/min at areas of widest path width. This modulation assumes that the layer thickness is inversely proportional to the feed rate and aims to result in an even path height. This allows the coating thickness to be controlled in a targeted manner despite the varying path width and opens up the possibility of thickness optimization, which is demonstrated here by applying a simple thickness gradient in the longitudinal direction of the demonstrator. This second path height modulation is achieved by remapping the first modulated feedrate data set from the original range of 3324–15,000 mm/min to the final range of 6781–15,000 mm/min.

The two ribbons on the sides of the pavilion segment are designed for a constant thickness of 30 mm, so the spray parameters—nozzle distance and feed rate—are also kept constant. The material thickness is achieved by stacking two layers of 15 mm at a feed rate of constant 4000 mm/min. The ribbon width of 40 mm is achieved by setting a minimal nozzle distance of 200 mm, resulting in an 80 mm path width (Table 1), that targets the outer edge of the ribbon, accepting to spray some of the material off target to respect the adjoining clean surface. From an alignment perpendicular to the surface, the nozzle orientation is rotated upwards by

30° around the respective path trajectory to keep the robot away from the ground and the concrete from spraying on the clean surface.

The order of spraying the individual surfaces is based on the envisioned surface texture. The surface articulation of the tween curves is given by the complex path planning of the large surfaces, so they will be sprayed after the ribbons are finished first. Lastly, a single trajectory was added to the robot path along the middle crease to join the two halves into a closed surface and to ensure that the pins on the middle frame element are fully embedded.

The main surfaces are intended to emphasise the properties of a shotcrete surface texture and demonstrate the ability of the rough and unpolished SC3DP process to articulate itself smoothly and delicately in its parametrically structured origin without postprocessing. Since the actual result of the surface cannot be predicted due to the novelty of such thin surfaces, the path planning must be repeatable as often as necessary to compensate for any unevenness that may occur. This is achieved by offsetting each plane of the path by its respective variable path height, multiplied by the number of layers. To achieve the thinnest possible coating on the textile formwork, each layer will be evaluated for structural and aesthetic adequacy before deciding whether an additional layer is necessary.

3.5.2 Preliminary tests for surface articulation

To achieve maximum slenderness, an experimental study of the coating's geometry and texture must be carried out as a preliminary test. The decisive parameters of these tests are the nozzle distance and the feed rate, as their interaction determines the geometry of the path cross-section and thus the thickness, evenness, and surface texture of the coating. To reproduce the texture of the formwork surface generated by Fibre Winding, additional fibres were wound onto the flat test bed, consisting of two screen-printed wooden panels measuring 2.5 × 1.25 m. Four robotic paths were planned on this test bed, corresponding to the same tween logic used in the demonstrator's path planning. The range of tween curve distances was also identical, scaled down to save space and material.

A parameter study on the variability of nozzle distance and feed rate was then carried out on the four different paths to determine whether the calculated parameters result in the desired real path geometries and how the variable calculations articulate on the surface texture. The selected parameter combinations for the four different test areas are listed in Table 2, with variations to isolate and evaluate specific influences.

The results of the preliminary tests show that the variability of the parameters is clearly reflected in the surface texture. When the nozzle distance parameter is varied (Area a), there is a noticeable increase in the visible path structure in the texture. If the feed rate is not variably adjusted in these cases, this effect intensifies, leading to sharp texture edges in the narrow areas where minimal nozzle distances occur (Fig. 13a).

In Area b, with a static nozzle distance and variable feed rate, the variable feed rate adjustment counteracts the high material build-up in narrow path regions, effectively equalising the material application height as expected (Fig. 13b). Conversely, in Area d, where both the nozzle distance and feed rate are static, the result is an overall flat and blurred surface texture (Fig. 13d).

Finally, in Area c, where both parameters are varied, the results show visible paths in the texture with a controlled material height, which counteracts the sharp edges and provides the intended surface articulation (Fig. 13c). This demonstrates that the dynamic adjustment of both nozzle distance and feed rate is essential for achieving control over the desired surface characteristics to be super thin, and delicate.

Table 2 List of parameters for preliminary tests

Area	Nozzle distance [mm]	Feed rate [mm/min]
a	Variable 400–850	Static 8000
b	Static 800	Variable 6781–15,000
c	Variable 400–850	Variable 6781–15,000
d	Static 800	Static 8000

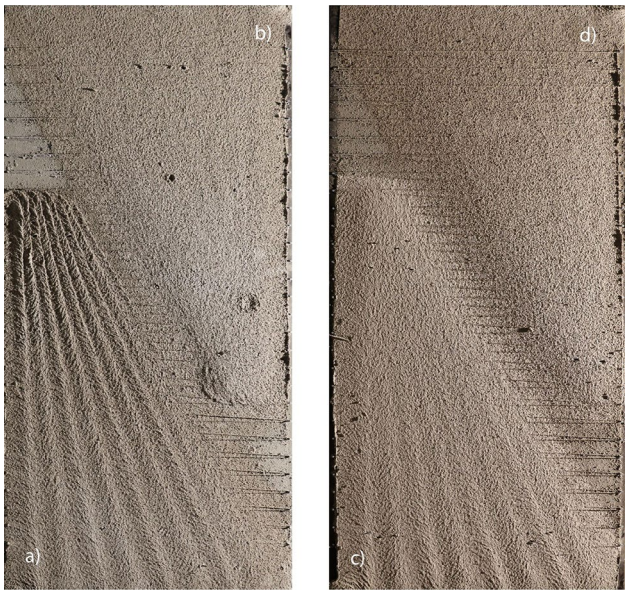

Fig. 13 Preliminary evaluation of RASP parameters—Influence on surface texturing

3.5.3 Path planning for green-state postprocessing

The concreting of the shell is followed by a single step of subtractive postprocessing to sharpen the outlines of the ribbons and smoothen the lateral surfaces on both sides, making them suitable for dry joint connexions. This is performed within a time window of about 3 h after the concrete is applied, when it is in green state, to achieve low tool abrasion and minimal machine time. For this green-state postprocessing, the CNC mill is equipped with a diamond grinding disc with a thickness of 5 mm and a radius of 210 mm, suitable for those 2-dimensional paths.

The milling path consists of only 3 points on each side, which form a polygonal chain on the outer edge of the demonstrator, with the start and end points in the extension of the path being 300 mm outside the cutting edges. The tool dimensions are taken into account by an offset from the edges of the demonstrator in the upward direction. The offset distance is 117 mm so that the saw blade has a minimal plunge depth but still plunges completely into the angle point of the path. The milling parameters are set at a spindle speed of 400 rpm and a feed rate of 1200 mm/min, but left open for manipulation in the process to be able to react to the material behaviour on demand.

4 Results

Based on the methodology described in the preceding sections, the real-scale demonstrator was fabricated. The observations collected during each process step are described in the following. In addition, an initial evaluation of the structural performance facilitated by this manufacturing approach is provided.

4.1 Real scale demonstrator fabrication

In preparation for the robotic fabrication steps, Fibre Winding, shotcrete application and post-processing, the steel frame was assembled manually with help of the robot arm pointing successively to the corners of the frame.

4.1.1 Observations robotic winding

In a first step, all Fibre Winding that did not require tape integration was performed (Fig. 14a). Manoeuvring the end effector between the pins requires sufficient accuracy, to avoid collisions with the frame but at the same time be close enough to the frame, so that the fibre strand does not slip off the pins or miss them at all. Due to the robot assisted frame positioning, the pins were surrounded accurately.

The robot's speed was manually adjusted to the production rate of the DWM, leading to a fabrication duration of 113 min for 161 m of reinforcement. Due to obligatory

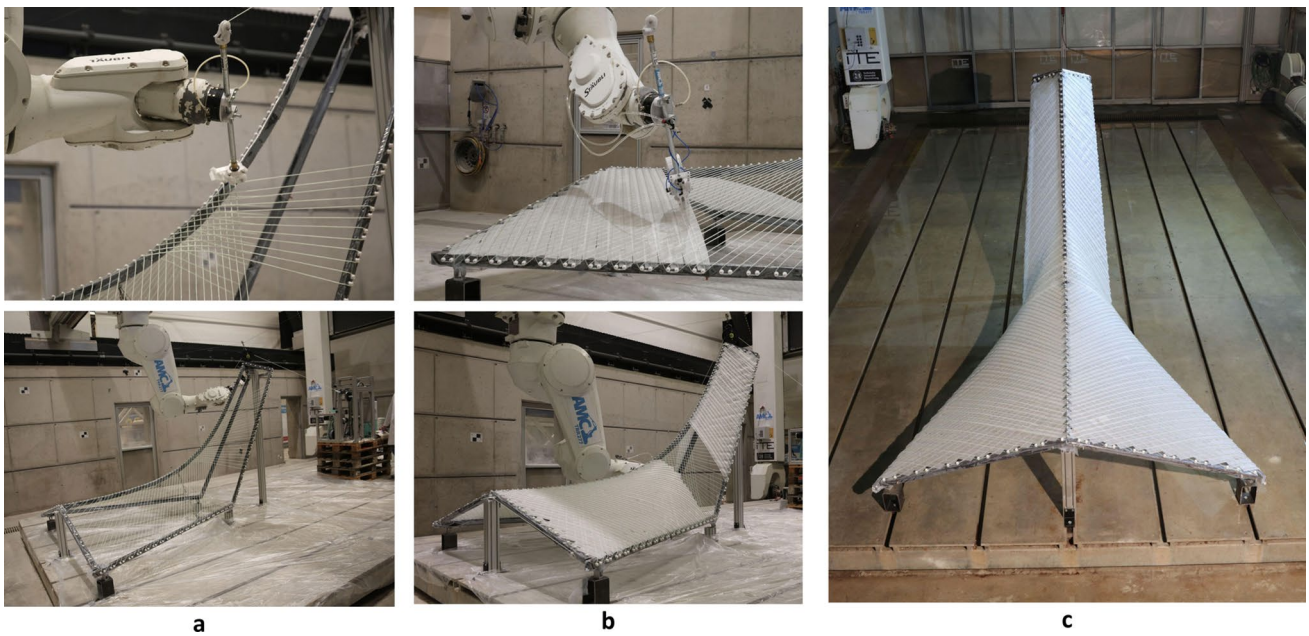

Fig. 14 Process sequence of robotic Fibre Winding: First, the frame is filled with fibre strands only (**a**) to create the basis for tape-enhanced winding (**b**), which results in a homogeneous surface across the entire frame (**c**)

cleaning of the DWM from epoxy resin debris, the tape enhanced winding was carried out the next day after the first fibre layer had hardened (Fig. 14b, c).

The accuracy of the geometric prediction could be inspected by the distance of the end effector to the mesh. As expected, minor deviations occurred due to bending of the initial fibre layer (Fig. 15a). A reduction of the distance between mesh and end effector could have facilitated more immediate and secure clamping of the tape amongst the fibres, enhancing the accuracy and stability of its placement.

In convex areas, the tape exhibited a more effective clamping action compared to flat regions, where adherence was still adequate. Nonetheless, minor defective corrugations were identified in flat regions, attributed to overfeeding of tape (Fig. 15b). Whilst the corresponding feeding mechanism would need to be revised, the cutting of the tape functioned reliably. The passive alignment of the end effector, balanced with a 4 kg counterweight on the DWM's dancer, functioned efficiently.

Discretization led to the formation of small triangular gaps along the edges (Fig. 15c). Selected significant gaps were manually filled. Laying a single tape lane along the edges could be an automated solution to compensate for this effect. The inclusion of tape extended the winding process duration to 192 min for 165 m of reinforcement, due to pauses for tape refilling and manual interactions when tape feeding failed.

4.1.2 Observations shotcrete and post-processing

After the robotic winding process was completed, the textile formwork was covered in plastic foil to protect it for a test run of concreting before the actual shotcrete layer was sprayed.

By that, it was observed that the tested parameters of the path planning actually translate to the expected concrete path dimensions which overlapped to a thin and even coating. With this validation, the fibre formwork was then uncovered and the same programme was restarted to perform the actual concreting process. It was started with the ribbons, which took 2:32 min on both sides for two shotcrete layers. Overshooting of material could not be avoided entirely, as the ribbons are too narrow to catch the whole spray width. The sprayed concrete filled the target area as expected, embedding the pins with no visible voids to the desired path thickness of minimum 30 mm evenly with minor amounts of excess material to be milled off later.

The most ambitious step of surface coating with variable nozzle distance and speed was started immediately after the spraying of the ribbons, when the already applied concrete was still in its fresh state (Fig. 16a). Other than expected from the test run on the plastic foil surface, it was observed that the path geometry was notably lower in width and did not distribute as fluently. This was assumed to occur due to the absorbent properties of the dry fleece tape, which did not allow the concrete to distribute as fluidly as it has on the smooth surface texture of the baseplate or the plastic foil used in the preliminary tests and test run. However, it was observed that the concrete coating still began to form a homogeneous coverage of the textile formwork, due to sufficient path overlap (Fig. 16b, c).

Furthermore, it was observed that holes were forming in the textile formwork during the surface coating process (Fig. 17a). Concrete was penetrating the overlapping seams of the tape, passing through and leaving the opened overlaps folded over to the backside of the surface. It was noticeable that the edge areas were particularly affected, but there were also occasional holes forming across the surface area. Although it could not be definitively clarified what caused

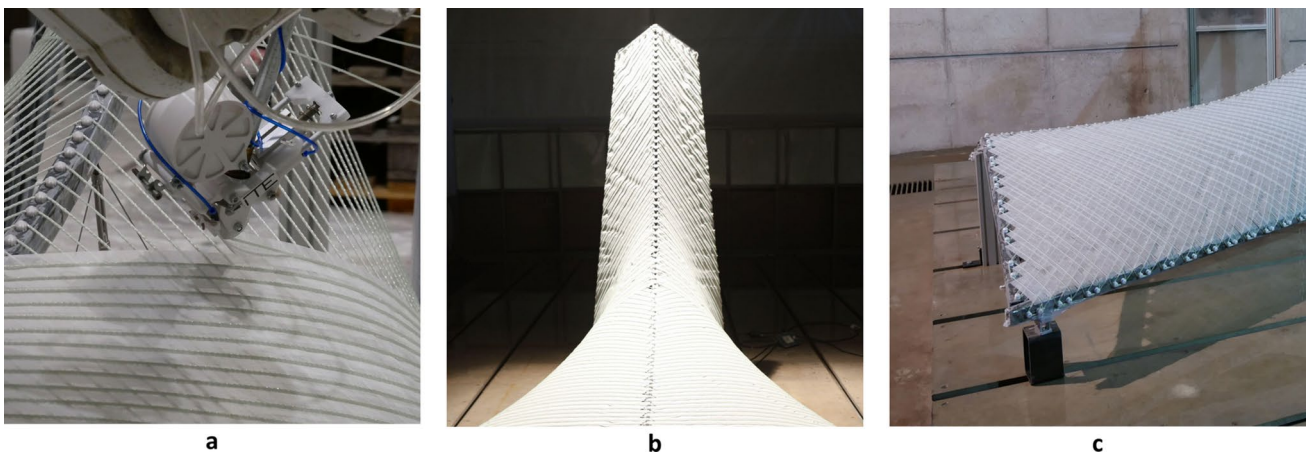

Fig. 15 Observations on winding with tape integration: **a** Increased distance between end effector and surface; **b** Highlighted corrugations of the tape in flat regions; **c** Triangular serrated edges of the tape surface due to discretisation

Fig. 16 **a** Pin embedding and filling of the ribbons by shotcrete; **b** RASP process on the double curved polysurface, **c** Surface articulation after completed RASP

Fig. 17 **a** Holes formed during RASP process as seen on the top side; **b** Visible aggregate separation

the holes to form, three likely factors were identified: The shotcrete impact due to a high air volume flow of 50 Nm3/h, which was necessary to apply the concrete to the target surface over the high nozzle distance, despite the spray angle, in a targeted manner. Second, the 2 mm grain size of the concrete used could have developed a projectile effect that penetrated the tape, as there was visible separation of aggregates (Fig. 17b). Lastly, the overlapping of the tape may not have been sufficient to withstand the shotcrete impact. This could be particularly the case near the tape endings, as most of the holes occurred near the borders of the demonstrator.

Despite complex robot movements, the path could be followed smoothly throughout the entire process. The major speed variations could be tracked without noticeable deviations caused by acceleration and deceleration. The subsequent second half of the surface proceeded equally satisfactorily as the first and was finalised with the central shotcrete path over the mid-axis after a process time of 6:09 min. The resulting surface rendered the desired surface articulation of the shotcrete process, with subtly recognisable parametric paths and a visible gradient of material thickness, which, in thinnest areas, revealed the fibre reinforcement in the texture.

The fibres and pins appeared to be well embedded already during the process, as it could be observed from the back that the tape was well absorbed by the applied concrete and no voids were visible on the fibres. This was confirmed by later investigations, in which the cured demonstrator was cut open to make the cross-section visible. As can be seen in Fig. 18b, no voids are visible in the cross-section, including the potential small spray shadow areas around fibres and pins.

Each of 36 measurements on cut-outs (compare Fig. 21a) resulted in an average thickness of 9.9 mm in the Base area and 6.8 mm in the top area with a standard deviation of 1.1 mm and 0.7 mm respectively. The systematic deviation from the target thicknesses of 8 mm and 4 mm can be partly explained by the relatively high

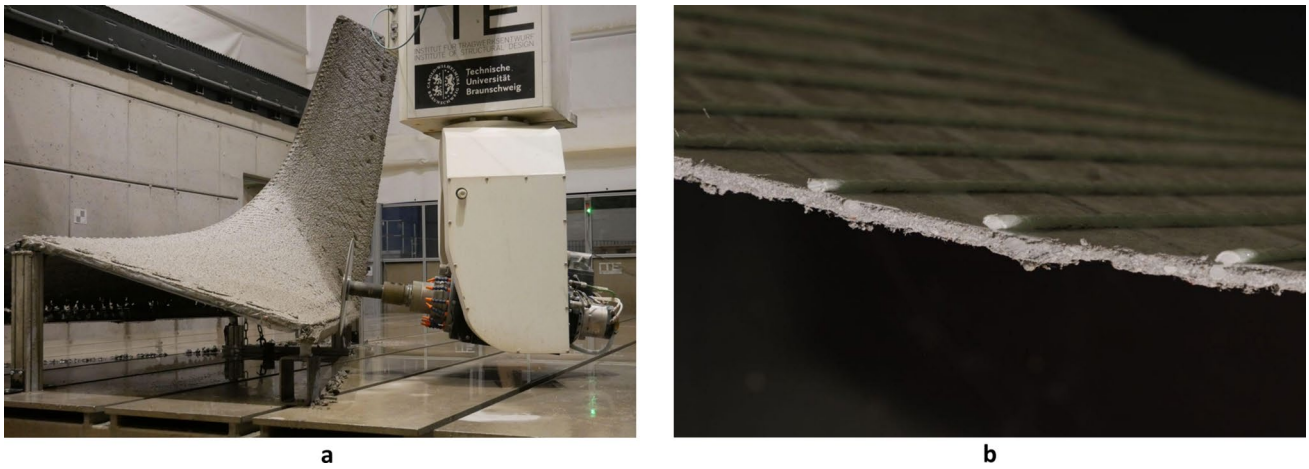

Fig. 18 **a** Green state postprocessing along the lateral edges; **b** Detailed view of a cutting edge with visible embedded fibres and soaked tape

surface roughness, as only the thickest areas are recorded by calliper measurements.

The last fabrication step of green-state postprocessing was started at 2:45 h of concrete age at the ribbons, so within the desired time window when the concrete was still in green state but kept his structure. This allowed for clean cuts without unintended material redistribution whilst the diamond milling disc could still travel quickly through it with minimal tool abrasion (Fig. 18a). This step took 8 min machine time for both sides. The machine time for the whole concreting process, including RASP of the main surface, and SC3DP and postprocessing of the ribbons adds up to 19 min in total. After the concrete was cured, the demonstrator was ready to be moved for erection and assembly.

4.1.3 Assembly, frame removal and joining

Originally, a thicker and double-sided concreting process was planned. However, as a proof of concept, this example has been limited to a thin, single-sided application of concrete. After curing, the demonstrator was rotated to its target orientation and placed on a pedestal that included four anchors tailored to the integrated connector plate (Fig. 19). Due to the undersized wall thickness, the metal frame was initially left within the structure.

The removability of the frame segments was assessed as part of partitioning the demonstrator for structural testing. Thanks to planning for disassembly, frame parts were able to be detached sequentially. High frictional resistance required increased force application to disengage the frame components. Only at thicker areas it was possible to remove them without causing damage. Building

Fig. 19 Crane-assisted assembly of the pavilion segment (**a**) onto a pedestal (**b**) by means of four tailored anchor bolts

on these insights, the frame system could be enhanced, for instance, through a pneumatic demoulding principle, making removal easier and non-destructive.

In addition, the joining concept was tested on two sections of the demonstrator, as depicted in Fig. 20. By extending the pin sleeves to through-holes, the connexion via bolts was facilitated. The machined concrete edges provided a flat contact surface for the join partners. However, due to variations in the shotcrete application thickness, the width of the contact surface varied significantly. Essentially, the usability of the pin sleeves for connexions was demonstrated. Yet, for a load-bearing connexion, specialised sleeves and a more controlled contact surface would be necessary.

4.2 Structural performance

Flexural tests have been conducted to investigate the influence of fabrication on the structural performance. Based on the demonstrator it was intended to identify the influence of the special characteristics of this fabrication method, particularly the role of the glass fibre fleece tape.

4.2.1 Sample overview and fabrication

So far, the function of the fibres for form-definition has been analysed, but they should also enable increased absorption of bending moments. 4-point flexural tests were therefore considered suitable for evaluation. DIN EN 12390 (En 2021) for testing hardened concrete and DIN 1170 (En 1998) for shot fibre reinforced concrete have been considered. However, the actual choice of

Fig. 20 Testing the joining principle on two cut-outs from the demonstrator: **a** Sectional view; **b** Detailed view of bolts

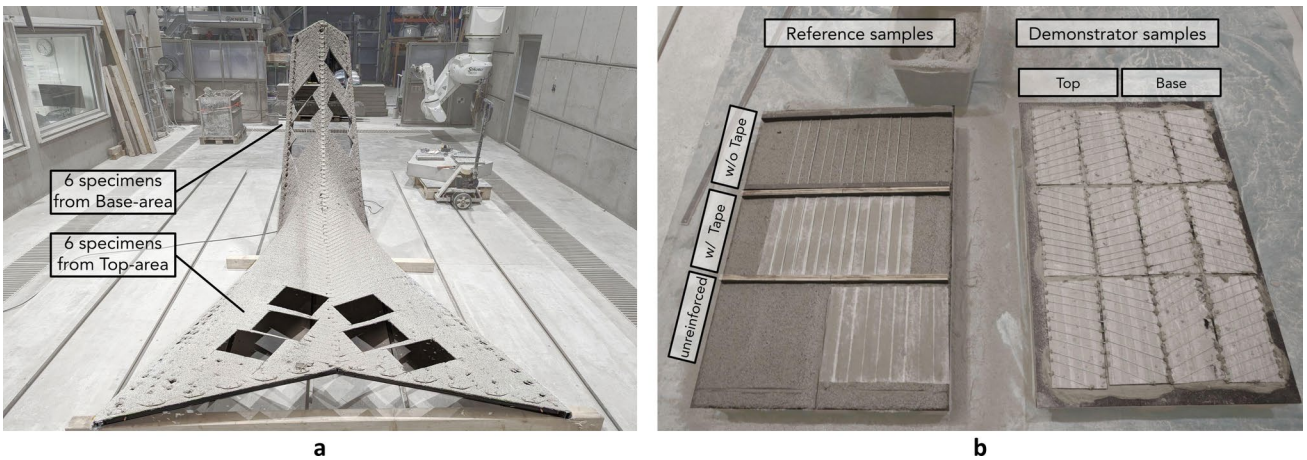

Fig. 21 **a** Location of cut-outs from the demonstrator; **b** Overview of specimen types for flexural testing

specimen design was driven by the geometry of the demonstrator. From two predominantly flat areas at the base and the top of the demonstrator, as marked in Fig. 21a, a total of 12 specimens could be retrieved, oriented along the embedded reinforcement fibre strands. With a size of 300 × 120 mm, three reinforcement fibre strands are located in each specimen.

The rear side of the demonstrator specimens, where no concrete was applied in the course of demonstrator fabrication, was retrospectively sprayed on by SC3DP using the same fine-grained polymer-modified cement–based concrete as for the front (Fig. 21b, right side).

As a reference, four further specimens were produced. Therefore, after printing a base layer with a target height of 10 mm, fleece tape and fibre strands of the same type as those in the demonstrator were inserted both separately and in combination (Fig. 21b, left side). After a break of 15 min, SC3DP was continued until the full specimen thickness was reached. Green state trowelling was used for all specimens to ensure that the desired thickness of 42 mm was achieved. The goal of this arrangement of configurations is to identify the influence of the fibre rebars, of the time sequence of concreting front and rear side and of the fleece tape on the bond.

4.2.2 Test results

After cutting the specimens to size, the depth of the reinforcement was measured as listed in Table 3, since it was noticed that, undesirably, the manufacturing led to significant variation of depth in a range between 27.3 and 37.5 mm. After 32 days, the specimens were tested in a universal testing machine with displacement control at 0.02 mm/s, a support spacing of 255 mm and a loading span at 1/3 of it (Fig. 22a). The additional bending in the centre was recorded with two LVDTs, the mean of which was added to the machine displacement for evaluation. It is worth noting that the centred measurement of displacement may not be representative in the case of asymmetrical crack development.

The force–displacement diagrams in Fig. 23 are used to compare the different reinforced configurations. As the specimens could not be produced according to the standard, the calculation of bending tensile stress is omitted. All specimens without rebars failed brittle, as expected. No influence of the fleece tape could be observed in these cases. The force at failure reached a maximum of 4.00 kN amongst the six unreinforced specimens. In comparison to the significantly higher resistance up to 11.04 kN of the reinforced specimens visible in Fig. 23, the effectiveness of the reinforcing bars is

Table 3 Dimensions of specimens; depth of reinforcement measured for all specimens (6 measurements each)

	Specimen count []	Minimum depth [mm]	Maximum depth [mm]	Mean depth [mm]	Full height (in the centre) [mm]	Width × length [mm]
Demonstrator base	6	32.3	35.5	34.5	41.0	120 × 300
Demonstrator top	6	36.0	37.5	36.7	39.6	120 × 300
Reference w/o tape	4	27.3	28.5	27.8	41.0	120 × 300
Reference w/ tape	4	28.8	29.8	29.1	41.3	120 × 300
Unreinforced	6	–	–	–	40.7	120 × 300

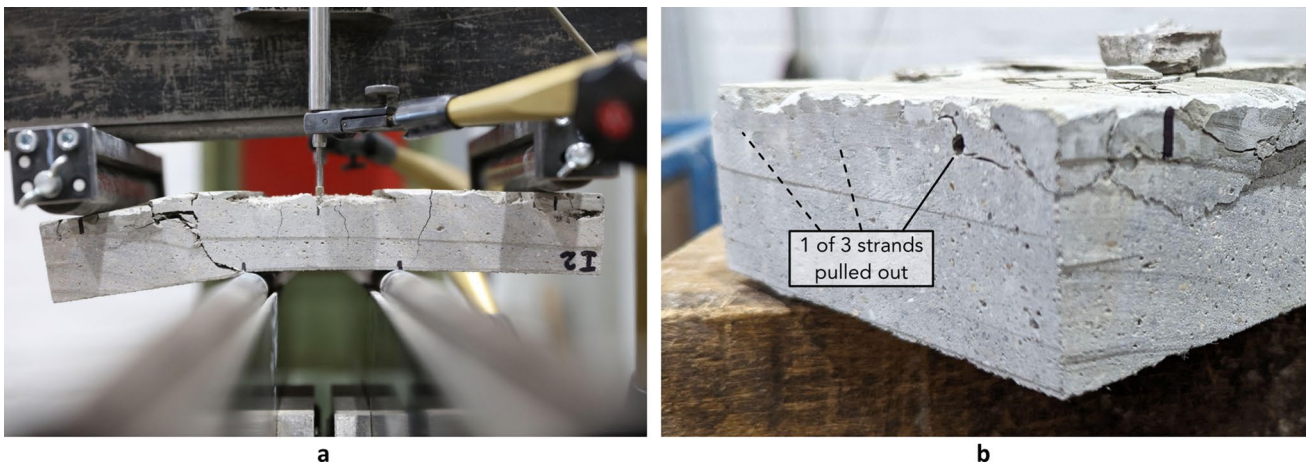

a b

Fig. 22 **a** Exemplary specimen from group "Demonstrator Top" exhibiting 4 cracks and slight delamination during 4-point flexural test; **b** Pull-out from the sides in the same specimen

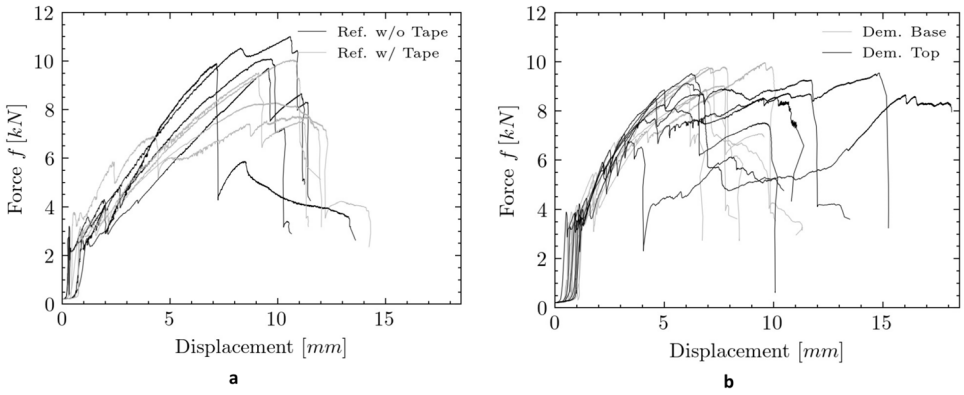

Fig. 23 **a** Force–displacement diagram of reinforced reference specimens with and without tape integration; **b** Force–displacement diagram of reinforced specimens from the demonstrators top and base area

fundamentally proven. The reinforced specimens had mostly three or four cracks similar to the ones visible in Fig. 22a. They extend beyond the loading span and can therefore be attributed to bending in the centre and to shear in the outer thirds.

For the reinforced specimens without tape, a linear behaviour until the consecutive rupture of the three rebars was observed. As typical for fibre reinforcement, a rather brittle than ductile failure occurred. When comparing the reference specimens that included tape, the graphs exhibit a more ductile behaviour with reduced maximum loads and slightly higher displacement. A moderate delamination behaviour along the tape occurred in all of the four specimens and could explain this behaviour as the rebars are located next to the tape. Thus, delamination could weaken the bond. However, pull-out from the sides was only observed in two of the specimens.

Interestingly, only half of the specimens from the demonstrator had cracks along the reinforcement. These were shorter (1–4 cm) and not always clearly identifiable as delamination. Due to the long time between concreting the front and the rear of the element a cold joint effect was expected. This, however, was more pronounced in the fresh-in-fresh printed references. It is assumed that the stronger delamination originated from the circumstance that the tape could not be sprayed from both sides for the reference specimens. Nevertheless, the maximum loads for the demonstrator specimens are lower than the reinforced reference without tape, although their effective depth of reinforcement was higher.

Meanwhile there are some inevitable differences between reference and demonstrator specimens, the two groups from the Base and the Top area of the demonstrator vary solely in the thickness of the concrete cover. The specimens from the top with a thinner concrete cover showed significantly higher displacement between 10 and 18 mm, meanwhile the other group from the Base area of the demonstrator failed rather brittle at a displacement between 7 and 10 mm. It is assumed that the extreme thin cover of the Top group has limited capacity to bond the reinforcement to the element. This hypothesis is supported by the observation of pull-out in four of six specimens of the Top group (Fig. 22b), meanwhile no pull-out was visible in the Base group.

Although in general, ductile behaviour is desirable, here it can be assumed that it appeared as a result of limited specimen length and weak embedding. Apart from that, the results are dominated by brittle failure, as is characteristic of continuous glass fibre.

To summarise, the production influences could not be isolated unambiguously and the comparability between the sample groups is limited, partly due to the varying effective depth. Although the highest load-capacity was achieved without tape, the results suggest that only minor impairments occur when spraying onto the tape from both sides with sufficient thickness. Even without using a bonding agent, there is no evidence to suggest that concreting on one side long after the opposite side has cured is disadvantageous.

5 Discussion

The fabrication method for thin reinforced concrete elements introduced here is both innovative and experimental. By applying this technique directly to a large, complex component (Fig. 24), several aspects were evaluated at once. However, it is crucial to acknowledge that this constitutes a first-time application, with some areas, such as structural design, not fully addressed.

5.1 Tailored process combination

The focus was primarily on digital fabrication, achieving full automation except for preparatory and finalising steps. The carefully tailored combination of textile formwork, fibre reinforcement and shotcrete created an efficient, waste-minimising process. Shotcrete proved suitable for embedding reinforcement, as indicated by the absence of spray shadows, and the potential corrosion resistance of fibre reinforcement

Fig. 24 The pavilion segment serves as a demonstrator for cutting-edge digital fabrication research. It highlights the potential of Robotic Fibre Winding for concrete construction, resulting in a structurally sound and visually compelling piece

makes it well-suited for thin concrete applications, such as achieved with the automated shotcrete process.

Preliminary tests revealed that thin shell components require additional formwork. The flexible adaptation of textile formwork complements fibre reinforcement well. In particular, the individual placement of tape has proven the ability to reproduce significant double-curvatures without folds. The tensioned fibre reinforcement, in turn, supports the limp fleece textile so efficiently that a formwork effect could be achieved with a material thickness of just 0.3 mm. Compared to conventional formwork, the material consumption is negligible, even when accounting for overlaps between tape lanes.

5.2 Challenges in the early development phase

Shotcrete and textile formwork are also well-matched, with the textile's porosity allowing for cement penetration whilst retaining the material apart from that. The spraying process proved beneficial for creating continuous surfaces by selecting appropriate parameters, demonstrating that a single-sided formwork is sufficient. However, the chosen glass fleece textile only withstands the shotcrete impact to a limited extent. Failures predominantly occurred near the borders, but no direct correlation to shotcrete parameters like nozzle distance was observed.

Adjusting the shotcrete impact through reduced aggregate size or airflow could prevent damage of the fleece. However, selecting an alternative textile material holds greater potential for improvement, especially when considering the decreased flexural strength observed in specimens containing fleece tape. A separation effect is assumed responsible, making textiles with higher porosity preferable. Replacing the fleece by a fine fibre glass mesh could yield sufficient resistance to shotcrete impact whilst not acting as separation layer but rather positively affecting structural behaviour as local reinforcement.

5.3 Fabrication informed design

Beyond structural and fabrication aspects, the form-defining process presented here is of particular interest. All components—frame, fibre reinforcement, textile, and concrete—contribute to the final shape to a certain extent. The frame explicitly sets boundaries that can be set freely by the designer. Yet, it needs to be considered that frame manufacturing and assembly are currently not part of the digital fabrication process. Exploring frame removability has opened up two options: reusability for similar shapes or designing frames as integral structural parts.

The surface within the frame is shaped by the mechanical nature of tensioned fibre strands. Simulating deposition behaviour allows for design incorporation including the influence of winding syntax. Yet, extending the simulation to elastic interaction of strands is expected to increase the accuracy of shape prediction. Although no significant deformation from fresh concrete weight was observed, this factor should be included in simulations.

Whilst the basic shape is determined by fibres and completed to a continuous surface by textile stripes, concrete application allows control over thickness distribution and surface articulation. The developed coating strategy proved applicable for complex non-rectangular surfaces. Whilst validated only on one side of the demonstrator, dual-sided concrete application could control reinforcement depth individually, accounting for varying bending stress within a component.

In contrast to earlier works (Gantner et al. 2022a; Rennen et al. 2023b), the concrete surface was deliberately left unfinished. As preliminary tests on surface articulation have shown, a homogeneous appearance is achieved in terms of colour, which appears smooth and true to geometry overall and exhibits a roughness in the order of magnitude of the largest grain (2 mm) in detail. Although this surface cannot be assigned to architectural concrete classes for cast concrete elements (Schulz 2023), some criteria, such as colour uniformity and evenness, are already satisfactorily met, if the defects caused by the fleece tape are excluded.

In this case study, an innovative manufacturing method revealed new shaping possibilities for filigree components. The material-efficient automated process promotes designs that follow the principle of "strength through form". The individualised allocation of reinforcement and concrete is the prerequisite for load-optimised element designs, so that thin roof shells or façade elements can be realised even with

high requirements to the load-bearing capacity when choosing appropriate materials like carbon fibre roving.

Whilst leading manufacturers of thin concrete elements like DUCON (Europe GmbH and Co 2024) rely on Ultra High Performance Concrete, in this case emphasis is placed on an economical and resource-saving manufacturing process through automation, which could lead to a wider application of concrete shells.

6 Outlook

To bridge the gap between the initial case study and practical construction, a more thorough examination of certain aspects of the fabrication method is essential. This includes exploring the role of the frames, particularly with a focus on joining techniques for element systems, as well as researching alternative textiles like fine glass fibre meshes for tape integration to improve compound quality. Eventually, sensor feedback could render the winding process more robust and increase control over the thickness of concrete application at both sides of the textile formwork.

Moreover, there is untapped potential for structural optimisation in the presented method, which can be further exploited by conducting in-depth investigations into design possibilities. At present, a two-step workflow is deemed suitable to optimise form and dimensioning respectively. The first step requires an improved form prediction regarding Frame Winding to account for its unique formal language in the optimization process. The universality of the robotic process steps allows for determining the appropriate sizing of reinforcement and concrete thickness independently in a second step. Compared to the realised demonstrator, an additional reinforcement layer can be provided in the future, with its strand orientation and strand materiality individually optimised.

Implementing these steps will consolidate this consistently digital construction approach, fostering a novel aesthetic of material-oriented processing and efficient form.

Supplementary Information The online version contains supplementary material available at https://doi.org/10.1007/s41693-025-00154-0.

Acknowledgements The research leading to these results received funding from the Collaborative research center TRR277 Additive Manufacturing in Construction (project number 414265976) and from Holcim Innovation Center. Open access funding was provided by Technische Universität Braunschweig. We acknowledge the active support from technicians and student assistants during experiments. We further acknowledge the creative input from students of the research associated course.

Author contribution Stefan Gantner*: Conceptualization, Investigation, Methodology, Software, Formal Analysis, Data curation, Writing—original draft, Writing review & editing, Visualization, Project administration. Philipp Rennen*: Conceptualization, Investigation, Methodology, Software, Data curation, Writing—original draft, Writing review & editing, Visualization, Project administration. Fatemeh Salehi Amiri: Conceptualization, Investigation, Writing—original draft. Tom Rothe: Investigation, Writing review & editing. Christian Hühne: Funding acquisition, Supervision, Writing review & editing. Dirk Lowke: Funding acquisition, Supervision, Writing review & editing. Harald Kloft: Funding acquisition, Supervision, Writing review & editing. Norman Hack: Conceptualization, Methodology, Funding acquisition, Supervision, Writing review & editing. *These authors contributed equally.

Funding Open Access funding enabled and organized by Projekt DEAL.

Data availability No datasets were generated or analysed during the current study.

Declarations

Conflict of interest The authors declare no competing interests.

References

Antuña Bernardo J (2006) The Evolution of the work of Eduardo Torroja: shell roofs with and without reinforcement rings. In: Proceedings of the Second International Congress on Construction History | International Congress on Construction History, Cambridge, pp 493–507

Ayres P, Leal da Silva WR, Nicholas P et al (2019) SCRIM—sparse concrete reinforcement in meshworks. Robot Fabric Archit Art des 2018:207–220. https://doi.org/10.1007/978-3-319-92294-2_16

Baek J, Deopurkar A, Redfield K (2007) Finding geodesics on surfaces

Bhat S, Kalthoff M, Shroeder P et al (2022) Textile reinforced concrete for free-form concrete elements: influence of the binding type of textile reinforcements on the drapability for manufacturing double-curved concrete elements. MATEC Web Conf 364:05019. https://doi.org/10.1051/MATECCONF/202236405019

Bhooshan S, Dell'Endice A, Ranaudo F et al (2024) Unreinforced concrete masonry for circular construction. Archit Intell 3:1–12. https://doi.org/10.1007/S44223-023-00043-Y

Block P, DeJong M, Davis L, Ochsendorf J (2010) Tile vaulted systems for low-cost construction in Africa. J Afr Technol Dev Forum (ATDF) 7:4–13

Block P, Schlueter A, Veenendaal D et al (2017) NEST HiLo: investigating lightweight construction and adaptive energy systems. J Build Eng 12:332–341. https://doi.org/10.1016/J.JOBE.2017.06.013

Block P, Van Mele T, Liew A et al (2018) Structural design, fabrication and construction of the Armadillo vault. Struct Eng 96:10–20. https://doi.org/10.56330/YSXL7244

Bodea S, Dambrosio N, Zechmeister C et al (2020) BUGA Fibre Pavilion: towards robotically-fabricated composite building structures. In: Fabricate 2020. UCL Press, pp 234–243

Carneau P, Mesnil R, Roussel N, Baverel O (2019) An exploration of 3d printing design space inspired by masonry. In: Proceedings of the IASS Annual Symposium 2019–Structural Membranes

Carneau P, Mesnil R, Roussel N, Baverel O (2020) Additive manufacturing of cantilever—from masonry to concrete 3D printing. Autom Constr 116:103184. https://doi.org/10.1016/J.AUTCON.2020.103184

Caron JF, Demont L, Ducoulombier N, Mesnil R (2021) 3D printing of mortar with continuous fibres: Principle, properties and potential for application. Autom Constr 129:103806. https://doi.org/10.1016/J.AUTCON.2021.103806

Caron J-F, Ducoulombier N, Demont L et al (2023) 3D printing of continuous-fibers cementitious composites. Open Conf Proc. https://doi.org/10.52825/OCP.V3I.193

Chaltiel S, Veenendaal D, Verzura F (2019) Terramia: drone-aided construction for a sustainable biobased housing prototype. In: Proceedings of IASS Annual Symposia. International Association for Shell and Spatial Structures (IASS), pp 1–8

Crosky A, Grant C, Kelly D et al (2015) Fibre placement processes for composites manufacture. Adv Compos Manuf Process des. https://doi.org/10.1016/B978-1-78242-307-2.00004-X

Dell'Endice A, Bouten S, Van Mele T, Block P (2023) Structural design and engineering of Striatus, an unreinforced 3D-concrete-printed masonry arch bridge. Eng Struct 292:116534. https://doi.org/10.1016/J.ENGSTRUCT.2023.116534

Demont L, Ducoulombier N, Mesnil R, Caron JF (2021) Flow-based pultrusion of continuous fibers for cement-based composite material and additive manufacturing: rheological and technological requirements. Compos Struct 262:113564. https://doi.org/10.1016/J.COMPSTRUCT.2021.113564

Demont L, Charrier M, Margerit P et al (2022) Flow-based pultrusion of anisotropic concrete: mechanical properties at hardened state. RILEM Bookseries 37:385–390. https://doi.org/10.1007/978-3-031-06116-5_57/FIGURES/5

Dittel G, Koch A, Gries T (2017) Innovative manufacturing methods of drapable textile reinforcements for folded/double curved concrete facade elements. In: International Conference on Advances in Construction Materials and Systems. pp 227–232

Dittel G, Scheurer M, Evers C et al (2023a) Structural performance of textile reinforced 3D-printed concrete elements. Open Conf Proc. https://doi.org/10.52825/OCP.V3I.429

Dittel G, Dringenberg S, Gries T (2023b) Through textile to reinforced 3D concrete printing. Lecture Notes Civ Eng 349:1094–1103. https://doi.org/10.1007/978-3-031-32519-9_110

Doerstelmann M, Knippers J, Menges A et al (2015) ICD/ITKE research pavilion 2013–14: modular coreless filament winding based on beetle elytra. Archit des 85:54–59. https://doi.org/10.1002/AD.1954

Dörrie R, Kloft H (2022) Force flow compliant robotic path planning approach for reinforced concrete elements using SC3DP. pp 370–375. https://doi.org/10.1007/978-3-031-06116-5_55

DIN EN (1998) 1170 – 1998 - 01 - Precast concrete products—Test method for glass-fibre reinforced cement

DIN EN (2021) 12390 – 2021 - 09 - Testing hardened concrete

Ercan Jenny S, Lloret-Fritschi E, Gramazio F, Kohler M (2020) Crafting plaster through continuous mobile robotic fabrication on-site. Constr Robot 4:261–271. https://doi.org/10.1007/S41693-020-00043-8

Ercan Jenny S, Lloret-Fritschi E, Jenny D et al (2022) Robotic plaster spraying: crafting surfaces with adaptive thin-layer printing. 3D Print Addit Manuf 9:177–187. https://doi.org/10.1089/3DP.2020.0355/ASSET/IMAGES/LARGE/3DP.2020.0355_FIGURE10.JPEG

Espion B (2016) Pioneering hypar thin shell concrete roofs in the 1930s. Beton- und Stahlbetonbau 111:159–165. https://doi.org/10.1002/BEST.201600001

Espion B (2018) Thin concrete shells by Eugène Freyssinet. In: 6th International Congress on Construction History (6ICCH 2018). Building Knowledge, Constructing Histories, pp 199–206

DUCON Europe GmbH & Co. KG, https://ducon.eu/, Accessed 29 Nov 2024

Friese D, Hahn L, Le Xuan H et al (2023) Robot-assisted manufacturing technology for 3D non-metallic reinforcement structures in the construction applications. Buildings 13:2748. https://doi.org/10.3390/BUILDINGS13112748

Gantner S, Rennen P, Rothe T et al (2022a) Core winding: force-flow oriented fibre reinforcement in additive manufacturing with concrete. pp 391–396. https://doi.org/10.1007/978-3-031-06116-5_58

Gantner S, Rothe T-N, Hühne C, Hack N (2022b) Reinforcement strategies for additive manufacturing in construction based on dynamic fibre winding: concepts and initial case studies. Open Conf Proc 1:45–59

Hack N (2018) Mesh Mould A robotically fabricated structural stay-in-place formwork system. ETH Zurich

Hack N, Dörfler K, Walzer AN et al (2020) Structural stay-in-place formwork for robotic in situ fabrication of non-standard concrete structures: a real scale architectural demonstrator. Autom Constr 115:103197. https://doi.org/10.1016/J.AUTCON.2020.103197

Hack N, Bahar M, Hühne C et al (2021) Development of a robot-based multi-directional dynamic fiber winding process for additive manufacturing using shotcrete 3d printing. Fibers. https://doi.org/10.3390/fib9060039

Iori T, Poretti S (2013) Pier Luigi Nervi: his construction system for shell and spatial structures. J Int Assoc Shell Spatial Struct 54:117–126

Janse van Rensburg J, Babafemi AJ, Combrinck R (2022) A textile reinforcement method for 3D printed concrete. MATEC Web Conf 364:05015. https://doi.org/10.1051/MATECCONF/202236405015

Kloft H, Hack N, Mainka J et al (2019) Additive Fertigung im Bauwesen: erste 3-D-gedruckte und bewehrte Betonbauteile im Shotcrete-3-D-printing-Verfahren (SC3DP). Bautechnik 96:929–938. https://doi.org/10.1002/BATE.201900094

Kloft H, Empelmann M, Hack N et al (2020a) Bewehrungsstrategien für den Beton-3D-Druck. Beton- und Stahlbetonbau 115:607–616. https://doi.org/10.1002/BEST.202000032

Kloft H, Krauss HW, Hack N et al (2020b) Influence of process parameters on the interlayer bond strength of concrete elements additive manufactured by Shotcrete 3D Printing (SC3DP). Cem Concr Res 134:106078. https://doi.org/10.1016/J.CEMCONRES.2020.106078

Kloft H, Sawicki B, Bos F et al (2024) Interaction of reinforcement, process, and form in digital fabrication with concrete. Cem Concr Res 185:107640

Lachmayer L, Böhler D, Freund N et al (2023) Modelling the influence of material and process parameters on Shotcrete 3D Printed strands—cross-section adjustment for automatic robotic manufacturing. Autom Constr 145:104626. https://doi.org/10.1016/J.AUTCON.2022.104626

Lee M, Mata-Falcón J, Popescu M, Kaufmann W (2023) Thin-walled concrete beams with stay-in-place flexible formworks and integrated textile shear reinforcement. Struct Concr 24:4960–4977. https://doi.org/10.1002/SUCO.202200648

Liew A, López DL, Van Mele T, Block P (2017) Design, fabrication and testing of a prototype, thin-vaulted, unreinforced concrete floor. Eng Struct 137:323–335. https://doi.org/10.1016/J.ENGSTRUCT.2017.01.075

Ludwig M (2017) "Formwork Virtuoso" Ulrich Müther (1934–2007), Exploring the Müther-Archive. In: Proceedings of IASS Annual Symposia. International Association for Shell and Spatial Structures (IASS). pp 1–10

Mechtcherine V, Michel A, Liebscher M et al (2019) Neue Carbonfaserbewehrung für digitalen automatisierten Betonbau. Beton- und Stahlbetonbau 114:947–955. https://doi.org/10.1002/BEST.201900058

Mechtcherine V, Michel A, Liebscher M, Schmeier T (2020) Extrusion-based additive manufacturing with carbon reinforced concrete: concept and feasibility study. Materials 13:2568. https://doi.org/10.3390/MA13112568

Mechtcherine V, Buswell R, Kloft H et al (2021) Integrating reinforcement in digital fabrication with concrete: a review and classification framework. Cem Concr Compos. https://doi.org/10.1016/j.cemconcomp.2021.103964

Van Mele T, Block P (2010) A novel form finding method for fabric formwork for concrete shells. In: J IASS proceedings of the annual IASS Symposium It is re

Méndez Echenagucia T, Pigram D, Liew A et al (2019) A cable-net and fabric formwork system for the construction of concrete shells: design, fabrication and construction of a full scale prototype. Structures 18:72–82. https://doi.org/10.1016/J.ISTRUC.2018.10.004

Neef T, Müller S, Mechtcherine V (2022) Integration of mineral impregnated carbon fibre (MCF) into fine 3D-printed concrete filaments. RILEM Bookseries 37:397–403. https://doi.org/10.1007/978-3-031-06116-5_59

Neef T, Mechtcherine V (2022) Simultaneous integration of continuous mineral-bonded carbon reinforcement into additive manufacturing with concrete. Open Conf Proc 1:73–81. https://doi.org/10.52825/OCP.V1I.80

Neef T, Dittel G, Scheurer M et al (2023) Utilizing textiles as integrated formwork for additive manufacturing with concrete. Lecture Notes Civ Eng 349:1285–1292. https://doi.org/10.1007/978-3-031-32519-9_130/FIGURES/6

Nerdinger W (2005) Frei Otto—complete works: lightweight construction—natural design. Birkhäuser

Nikravan A, Aydogan OG, Dittel G et al (2023) Implementation of continuous textile fibers in 3D printable cementitious composite. Lecture Notes Civ Eng 349:1243–1252. https://doi.org/10.1007/978-3-031-32519-9_126

Nuh M, Oval R, Orr J, Shepherd P (2022) Digital fabrication of ribbed concrete shells using automated robotic concrete spraying. Addit Manuf 59:103159. https://doi.org/10.1016/J.ADDMA.2022.103159

Oval R, Costa E, Thomas-Mcewen D, et al (2020) Automated framework for the optimisation of spatial layouts for concrete structures reinforced with robotic filament winding. In: Proceedings of the 37th International Symposium on Automation and Robotics in Construction, ISARC 2020: From Demonstration to Practical Use—To New Stage of Construction Robot, pp 1541–1548. https://doi.org/10.22260/ISARC2020/0214

Popescu MA (2019) KnitCrete: stay-in-place knitted formworks for complex concrete structures

Popescu M, Reiter L, Liew A et al (2018) Building in concrete with an ultra-lightweight knitted stay-in-place formwork: prototype of a concrete shell bridge. Structures 14:322–332. https://doi.org/10.1016/J.ISTRUC.2018.03.001

Popescu M, Rippmann M, Liew A, et al (2019) Concrete shell built using a cable-net and knitted formwork. In: Structure Published by Detail. https://www.detail.de/artikel/betonschale-aus-stahlseilen-und-gestrickter-schalung-33857/. Accessed 26 Nov 2021

Popescu M, Rippmann M, Liew A et al (2021) Structural design, digital fabrication and construction of the cable-net and knitted formwork of the KnitCandela concrete shell. Structures 31:1287–1299. https://doi.org/10.1016/J.ISTRUC.2020.02.013

Prado M, Dörstelmann M, Schwinn T et al (2014) Core-less filament winding. In: Robotic fabrication in architecture, art and design 2014. Springer International Publishing, pp 275–289

Prado M, Dörstelmann M, Menges A, et al (2017) Elytra filament pavilion: robotic filament winding for structural composite building systems. In: Fabricate 2017. UCL Press, pp 224–231

Ranaudo F, van Mele T, Block P (2021) A low-carbon, funicular concrete floor system: design and engineering of the HiLo floors. In: IABSE Congress, Ghent 2021: structural engineering for future societal needs 2016–2024. https://doi.org/10.2749/GHENT.2021.2016

Rennen P, Khader N, Hack N, Kloft H (2023a) A hybrid additive manufacturing approach. In: Proceedings of the 41st annual conference of the association of computer aided design in architecture (ACADIA), pp 428–437. https://doi.org/10.52842/CONF.ACADIA.2021.428

Rennen P, Gantner S, Dielemans G et al (2023b) Robotic knitcrete: computational design and fabrication of a pedestrian bridge using robotic shotcrete on a 3D-Knitted formwork. Front Built Environ 9:4. https://doi.org/10.3389/FBUIL.2023.1269000

Rippmann M (2016) Funicular shell design: geometric approaches to form finding and fabrication of discrete funicular structures

Rippmann M, Liew A, Van Mele T, Block P (2018) Design, fabrication and testing of discrete 3D sand-printed floor prototypes. Mater Today Commun 15:254–259. https://doi.org/10.1016/J.MTCOMM.2018.03.005

Rothe T, Gantner S, Hack N, Hühne C (2023a) A dynamic winding process of individualized fibre reinforcement structures for additive manufacturing in construction. Open Conf Proc. https://doi.org/10.52825/OCP.V3I.187

Rothe T, Pösch J, Gantner S, et al (2023b) Optimization of tensile properties and bond behaviour to concrete of fibre reinforcement strands produced within a dynamic fibre winding process. In: 11th International Conference on Fiber-Reinforced Polymer (FRP) Composites in Civil Engineering (CICE 2023)

Scheerer S, Chudoba R, Garibaldi MP, Curbach M (2017) Shells made of textile reinforced concrete-applications in Germany. J Int Assoc Shell Spatial Struct 58:79–93. https://doi.org/10.20898/J.IASS.2017.191.846

Schinegger K, Rutzinger S, Ladinig J, Li M (2020) Becoming structure. In: Impact: design with all senses, pp 214–223. https://doi.org/10.1007/978-3-030-29829-6_17

Schulz, J. (2023). Merkblätter mit Sichtbeton-Relevanz. In: Sichtbeton. Springer Vieweg, Wiesbaden. https://doi.org/10.1007/978-3-8348-2250-5_3

Schützeichel R, Beckh M, Ruiz-Funes J, et al (2020) Candela Isler Müther. Positions on Shell Construction. Birkhäuser

Solly J, Frueh N, Saffarian S, et al (2018) ICD / ITKE Research Pavilion 2016/2017: Integrative design of a composite lattice cantilever. In: IASS 2018 Creativity in Structural Design

Solly J, Knippers J, Dörstelmann M (2020) Coreless filament winding: from academia to practice. In: design transactions: rethinking information modelling for a new material age. UCL Press, pp 114–121

Stadler P (2014) Curve shortening by short rulers. ESAIM Proc Surv 46:217–232. https://doi.org/10.1051/PROC/201446018

Taha N, Walzer AN, Ruangjun J, et al (2019) Robotic AeroCrete—a novel robotic spraying and surface treatment technology for the production of slender reinforced concrete elements. In: Architecture in the Age of the 4th Industrial Revolution—Proceedings

of the 37th eCAADe and 23rd SIGraDi Conference. CumInCAD, pp 245–254

Tsarkova LA, Bahners T, Zhu X et al (2023) Current and future trends in textiles for concrete construction applications. Textiles 3:408–437. https://doi.org/10.3390/TEXTILES3040025

Veenendaal D, Block P (2014) Design process for prototype concrete shells using a hybrid cable-net and fabric formwork. Eng Struct 75:39–50. https://doi.org/10.1016/J.ENGSTRUCT.2014.05.036

Veenendaal D, West M, Block P (2011) History and overview of fabric formwork: using fabrics for concrete casting. Struct Concr 12:164–177. https://doi.org/10.1002/SUCO.201100014

Veenendaal D, Bakker J, Block P (2017) Structural design of the flexibly formed, meshreinforced concrete sandwich shell roof of nest hilo. J Int Assoc Shell Spatial Struct 58:23–38. https://doi.org/10.20898/J.IASS.2017.191.847

Yang HQ, Klug C, Schmitz TH (2023) Fiber-re inforced clay: an exploratory study on automated thread insertion for enhanced structural integrity in LDM. Ceramics 6:1365–1383. https://doi.org/10.3390/CERAMICS6030084/S1